**TITLE**

# Revealing function-altering MECP2 mutations in individuals with autism spectrum disorder using yeast and *Drosophila*.

**AUTHOR LIST**

Eric Chen[1]*, Jessica Schmitt[1]*, Graeme McIntosh[1]*, Barry P. Young[1], Tianshun Lian[1], Jie Liu[1], Kexin K. Chen[2], J. Beatrice Liston[1], Lily MacDonald[1], Bill Wang[1], Sonia Medina Giro[1], Benjamin Boehme[1], Mriga Das[1], Seevasant Indran[1], Jesse T. Chao[3], Sanja Rogic[2], Paul Pavlidis[2], Douglas W. Allan[1]#, and Christopher J.R. Loewen[1]#

[1] Department of Cellular and Physiological Sciences, The Life Sciences Institute, The University of British Columbia, 2350 Health Sciences Mall, Vancouver, BC, Canada, V6T 1Z3

[2] Department of Psychiatry and Michael Smith Labs, The Michael Smith Institute, The University of British Columbia, 301-2185 East Mall, Vancouver, BC, Canada, V6T 1Z4

[3] Department of Medical Biophysics, Sunnybrook Research Institute, The University of Toronto, 2075 Bayview Avenue, E240, Toronto, Ontario, Canada, M4N 3M5

(co-first *, co-corresponding **#)**

(email: christopher.loewen@ubc.ca, doug.allan@ubc.ca)

Running title: Altered MECP2 function in autism

Keywords: MECP2, autism spectrum disorder, ASD, Rett syndrome, variant prediction, budding yeast, Drosophila, genetic interactions, Sentinel Interaction Mapping, VariCarta, transgenesis

## ABSTRACT

Pathogenic variants in MECP2 commonly lead to Rett syndrome, where MECP2's function as a DNA cytosine methylation reader is believed critical. MECP2 variants are also catalogued in individuals with autism spectrum disorder (ASD), including nine missense variants which had no known clinical significance at the start of this study. To assess these nine variants as risk alleles for ASD, we developed MECP2 variant functional assays using budding yeast and *Drosophila*. We calibrated these assays with known pathogenic and benign variants. Our data predict that four ASD variants are loss of function and five are functional. Protein destabilization offers insight into the altered function of some of these variants. Notably, yeast and *Drosophila* lack DNA methylation, yet all Rett pathogenic and ASD variants located in the methyl DNA binding domain that we analyzed proved to be loss of function, suggesting a clinically-relevant role for non-methyl DNA-binding by MECP2.

## INTRODUCTION

The X-linked protein MECP2 was first identified in screens for proteins recruited to methylated DNA (Lewis et al. 1992), and loss of function (LoF) alleles of MECP2 were subsequently found as causative in the neurodevelopmental disorder, Rett syndrome (Amir et al. 1999). Since then variants in MECP2 have been found in most cases of Rett, but also in other neurodevelopmental disorders, including autism spectrum disorder (ASD) (Wan et al. 1999; Amir et al. 2000; Nomura 2005; Chahrour and Zoghbi 2007). The origin and phenotypic consequence of MECP2-damaging variants differ notably between sexes. In females, the vast majority of these variants are *de novo*, while in males, they can also be inherited from unaffected mothers (Ananth et al. 2024). Variants that typically result in Rett syndrome in females tend in males to cause severe

47 neonatal encephalopathy, often leading to death in the first year of life. However, in males with
48 two populations of X chromosomes, such as those with Klinefelter syndrome (47XXY) or
49 somatic mosaicism, these variants result in a milder Rett-like condition known as male RTT
50 encephalopathy. Males can also be affected by variants that are seemingly benign in females,
51 which can lead to moderate to severe intellectual disability (Pascual-Alonso et al. 2021).
52
53 MECP2 has largely been examined as a DNA cytosine methylation reader via its methyl cytosine
54 binding domain (MBD) that recruits co-repressor complexes to DNA to repress transcription via
55 its transcriptional repressor domain (TRD) (Jones et al. 1998; Ng and Bird 1999; Lunyak et al.
56 2002; Harikrishnan et al. 2005). The MBD, and to a lesser extent the TRD, harbors most Rett
57 LoF variants (Ehrhart et al. 2021), resulting in variants which are believed to reduce binding to
58 methylated DNA or reduce recruitment of co-regulator complexes, respectively (Ballestar et al.
59 2000; Yusufzai and Wolffe 2000). While numerous MECP2 variants have been found in patients
60 that exhibit Rett with ASD, recent reports have annotated five MECP2 missense variants in ASD
61 without an associated Rett diagnosis (R91W, G195S, A202G, E282G, S411R) (Schaaf et al.
62 2011; Wang et al. 2016; Wen et al. 2017; Guo et al. 2018; Leblond et al. 2021). However, it is
63 unclear whether any of these variants are function altering and clinically significant. Two of
64 them, R91W and A202G, are classified by ClinVar (Landrum et al. 2018) as variants of
65 uncertain significance (VUS) in cases of severe neonatal onset encephalopathy with
66 microcephaly. E282G is classified by ClinVar as likely pathogenic. The remaining two variants
67 (G195S and S411R) have no current ClinVar classification.
68

69 While MECP2 is understood to primarily be a methyl-cytosine DNA (DNAm) binding protein, it
70 has become clear it also binds unmethylated DNA with a preference for GC-rich sequences
71 (Georgel et al. 2003; Hansen et al. 2010; Skene et al. 2010; Cheng et al. 2014). This has been
72 proposed as an alternate hypothesis for why MECP2 appears to preferentially bind methylated
73 GC-rich regions of the genome, as opposed to binding DNAm methylation *per se*. It can be
74 challenging to segregate DNAm-dependent from DNAm-independent functions of MeCP2 *in*
75 *vivo*, as DNAm is both abundant and essential in mammals. Consequently, it is still unclear what
76 fraction of MeCP2's functions are dependent on its interaction with methylated and/or
77 unmethylated DNA. Such ambiguity leaves unresolved the question of whether disease relevant
78 variants in MECP2 selectively disrupt binding to methylated versus unmethylated DNA.
79
80 There are extremely low levels of methylated cytosine in the *Drosophila* genome, and none in
81 *Saccharomyces cerevisiae* (Lyko et al. 2000; Buitrago et al. 2021). Thus, fly and yeast offer
82 avenues to explore the interactions of MECP2 with unmethylated DNA, and to test if Rett and
83 ASD variants alter MECP2 binding to unmethylated DNA. Moreover, while neither organism
84 has an ortholog of *MECP2*, both organisms are robust genetic models that have proven well
85 suited to comparing the function of large numbers of gene variants (Post et al. 2020; Young et al.
86 2020; Ganguly et al. 2021; Her et al. 2024). MECP2 has been expressed in *Drosophila*, where it
87 associates with chromatin and mediates transcriptional repression via interactions with orthologs
88 of known MECP2 physical interactors in humans, including Sin3A, N-CoR, REST as well as
89 other chromatin modifiers (Cukier et al. 2008). In fly neurons, MECP2 impacts dendritic
90 branching and behavioural output (Vonhoff et al. 2012; Williams, White, et al. 2016) and C-
91 terminal truncation mutants (R294X specifically) promote neuronal apoptosis (Williams, Mehler,

92 et al. 2016). In yeast, MECP2 has recently been shown to bind chromatin and mediate
93 widespread transcriptional repression (Brown et al. 2025 Mar 18).

94 Our goal in this study was to use the *Drosophila* and budding yeast models to test the functional
95 impact of these ASD MECP2 variants to determine whether they may confer autism risk, by
96 virtue of their altered function. We calibrated our assays with MECP2 variants classified by
97 ClinVar as pathogenic or benign, in accordance with American College of Medical Genetics and
98 Genomics (ACMG) guidelines for experimental assays (Brnich et al. 2019); first to validate our
99 assays for variant assessment, and second to provide a rubric for determining if test ASD variants
100 are likely pathogenic or likely benign. All calibration variants functioned as expected in the
101 *Drosophila* assay, indicating that we could functionally assess any test variants. The yeast assay
102 could be calibrated appropriately for the MBD domain, but the MBD proved to be the only
103 domain showing the expected separation between benign and pathogenic calibration variants.
104 Our analyses indicate four of the nine test ASD variants were LoF, making these variants
105 candidate risk alleles for ASD. Interestingly, these variants mostly proved to be less severe LoF
106 than Rett-associated pathogenics, providing a possible explanation for how MECP2 mutations
107 can lead to ASD, but not Rett.

108

109 **METHODS**

110 **MECP2 isoform selection**

111 *MECP2* has two major isoforms, E1 and E2. We selected to work with *MECP2* isoform E2
112 (ENST00000303391, NM_004992) based on the recommendation by the ClinGen
113 Rett/Angelman-like Expert Panel (McKnight et al. 2022). This transcript is annotated as the

114 APPRIS (Annotation of Principal and Alternative Splice Isoforms (Rodriguez et al. 2013))
115 principal isoform in Ensembl genome browser, based on the annotations for protein structure,
116 function and cross-species conservation, and is the highest expressed transcript in the brain
117 (GTEx portal; **gtexportal.org**).
118

119 **Variant aggregation, annotation and prioritization**

120 We utilized our in-house computational pipeline to aggregate *MECP2-E2* missense variants from
121 ClinVar and VariCarta and perform comprehensive annotation. We collected ClinVar variants
122 (downloaded in January 2022) that have at least one gold review star, i.e., the review status
123 (CLNREVSTAT) has to have one of the following designations: "criteria provided, single
124 submitter", "criteria provided, conflicting interpretations", "criteria provided, multiple
125 submitters, no conflicts" or "reviewed by expert panel". For each of these variants, we also
126 obtain its interpretation (clinical significance; CLNSIG) and reported condition (disease name;
127 CLNDN). The ASD missense variants were obtained from VariCarta, a database of variants
128 found in individuals diagnosed with ASD and reported in the scientific literature, that we created
129 (Belmadani et al. 2019). We annotated the aggregated variants using the Ensembl VEP tool
130 (McLaren et al. 2016). We also added protein domain annotation relevant in the context of Rett
131 Syndrome (Good et al. 2021).
132

133 ***MECP2-E2* cloning**

134 A *MECP2-E2* cDNA clone was obtained (Horizon, Clone Id: 3956518, # MHS6278-
135 202830559), and *MECP2* coding sequences were amplified with iProof DNA polymerase (Bio-
136 Rad, California USA, #1725301) using the following primers:

137 GA-attL1-MECP2-522-F (tgtacaaaaaagcaggctccggcaccatggtagctgggatgttag)

138 GA-attL1-MECP2-522-R (ttgtacaagaaagctgggtctatcagctaactctctcggtc)

139 Amplicons were cloned in PCR8-GW-TOPO (Invitrogen, ThermoFisher Scientific, Waltham,

140 USA, catalog #K250020) using NEBuilder HiFi DNA Assembly Master Mix (New England

141 Biolabs, USA, # M5520). The resulting construct was named MECP2-pENTRY. A sequence of

142 CCGGCACC was introduced in primer GA-attL1-MECP2-522-F (underlined) preceding the

143 start codon for *MECP2-E2*. After LR cloning of MECP2-pEntry into pDEST vectors, this

144 CCGGCACC sequence can function as a Kozak sequence to initiate translation, or as an in-

145 frame linker for N-terminal peptide sequences. Missense variants were generated in MECP2-

146 pENTRY either using the Q5 mutagenesis kit (New England Biolabs, USA, # E0554) in house,

147 or were made by GenScript (New Jersey, USA). For MECP2 expression clone construction,

148 MECP2-pENTRY plasmids were subcloned in pAG426GAL-ccdB (a kind gift from a gift from

149 Susan Lindquist; Addgene plasmid # 14155) or pGW-HA.attB (Bischof et al. 2007) using the

150 Gateway LR Clonase reaction (Thermo Fisher Scientific, Waltham, USA, catalog # 11791020).

151 All transgenic *UAS-MECP2* variants (on pGW-HA.attB) *Drosophila* strains used were verified

152 by Sanger sequencing (UBC NAPS, Vancouver, Canada) or whole amplicon sequencing

153 (Plasmidsaurus, CA, USA) (Supplemental Data 1).

154

155 **Sentinel interaction mapping (SIM) in yeast**

156 SIM screening for *MECP2* was performed as described previously (Young et al. 2020). A singer

157 RoToR HDA colony arraying robot was used to copy arrays of yeast cells. All steps were

158 performed at a density of 1,536 colonies per plate and plates were incubated for 24 hours at 30

159 °C prior to the next pinning step, except where indicated otherwise. The SGA query yeast strain

160 Y7092 (Tong et al. 2001) was transformed with plasmid pSI7338-MECP2 and arrayed on
161 synthetic defined medium lacking uracil. The haploid yeast deletion mutant array (DMA) was
162 arrayed across a total of four plates on YPD medium containing 200 mg/L G418 sulfate
163 (YPD+G418). The query array was mated to the DMA by subsequently pinning both arrays on to
164 fresh YPD plates. Diploids were selected by pinning colonies to synthetic defined medium
165 lacking uracil containing 200 mg/L of G418 sulfate and subsequently pinned to YPD+G418
166 plates. Each plate was then pinned in triplicate to enriched sporulation media (Tong et al. 2001)
167 and incubated at 22 °C for seven days. Following this, *MAT*a haploid cells were germinated by
168 pinning to synthetic complete medium lacking histidine, arginine and lysine with the addition of
169 50 mg/L canavanine sulfate, 50 mg/L thialysine and incubating for two days. To select for
170 deletion strains carrying the MECP2-Ref plasmid, colonies were pinned to two pairs of plates
171 ("control" and "experimental") containing synthetic complete medium lacking histidine,
172 arginine, lysine and uracil, containing 50 mg/L canavnine sulfate, 50 mg/L thialysine, 200 mg/L
173 G418 sulfate ("HURK+G418" medium). The experimental set was supplemented with 10 nM -
174 estradiol to induce expression of *MECP2*; this was omitted from the control set. The final plates
175 used for imaging were generated by copying each of these plates once more to the same medium.
176 Plates were scanned using a CanoScan 8600F flatbed scanner and subsequently analyzed using
177 *Balony* software (Young and Loewen 2013) to compare the normalized colony size for each
178 strain in the presence or absence of estradiol. Genetic interactions were defined as those strains
179 where the ratio of experimental:control colony size was below a threshold determined by *Balony*
180 in all three replicates and with a p-value $< 0.05$. The strains *pho85*Δ*, rad50*Δ*, slx5*Δ*, swi4*Δ*,*
181 *swi6*Δ*,* and *xrs2*Δ were confirmed to be correct by PCR amplification of down-tag barcodes with
182 the standard primers B-U1 and B-D1 and sequencing.

183

184 **Yeast quantitative liquid growth assays**

185 Yeast strain JHY716 was transformed with various plasmids containing *MECP2* variants placed
186 downstream of the *GAL1* promoter. Four independent clones were picked from transformation
187 plates and transferred to SD-URA media containing 2% raffinose, 2% galactose to induce
188 expression of *MECP2*. For each clone, a 2 mL culture in SD-URA with 2% raffinose, 2%
189 galactose was grown overnight at 30 °C in a shaking incubator. The following morning, cultures
190 were diluted to an OD600 of ~0.25 in the same media. After 6 hours of incubation at 30 °C, log
191 phase cultures were diluted to an OD600 of 0.125. Three aliquots of 200 µl were taken from each
192 culture and transferred to a well of a flat-bottomed 96-well dish. Growth of cultures was
193 measured overnight at 30 °C with shaking at 800 rpm in an Agilent Logphase 600 plate reader.
194 All plates contained strains expressing wild type *MECP2* and the corresponding empty vector as
195 controls. The exponential growth constant k was determined for each well by fitting to an
196 exponential growth equation during the exponential phase (typically between 5 and 10 hours post
197 dilution).

198

199 **Protein abundance assays**

200 To determine the abundance of MECP2 variants in yeast, strains were grown in SD-URA media
201 containing 2% raffinose to early log phase. MECP2 expression was induced by the addition of
202 2% galactose to the growth medium. Cells were harvested three hours later by centrifugation and
203 stored at -80 °C for subsequent processing. Cell pellets were resuspended in Laemmli sample
204 buffer, and heated to 95 C for 5 minutes. Cell lysis was achieved by the addition of 50 µl acid-
205 washed glass beads followed by two rounds of disruption in a MP Biomedical FastPrep-24

206 homogenizer (maximum speed for 60 s with 5 minutes cooling between cycles). Samples (0.2
207 OD600 equivalents) were separated by SDS-PAGE on Bio-Rad 4-15% pre-cast gels and
208 transferred to nitrocellulose membranes. MECP2 was immunoblotted using Sigma antibody
209 (M9317), with PGK1 (Abcam AB113687) used as a loading control. For visualization,
210 secondary antibodies conjugated to Cy3 (MECP2) and AlexaFluor-488 (PGK1) were used and
211 imaged using a Bio-Rad ChemiDoc MP Imaging System. MECP2 band volume was normalized
212 to PGK1 band volume for each variant.
213
214 ***Drosophila* strains**
215 All flies were maintained on standard cornmeal food at 25 °C and 70% humidity unless
216 otherwise specified. *P{GAL4}A9* (BL8761) (referred to as *A9-GAL4*) was obtained from
217 Bloomington *Drosophila* Stock Centre (Indiana, USA). *UAS-MECP2* reference (*UAS-MECP2-*
218 *ref*) and variant sequences (collectively termed *UAS-MECP2.#*) were integrated into embryos of
219 genotype *y[1] w[] P{y[+7.7]=nos-phiC31\int.NLS}X; P{y[+t7.7]=CaryP}attP40* (referred to as
220 attP40) by Genome ProLab (Quebec, Canada), and maintained as *w[1118]; P{y[+t7.7]*
221 *w[+mC]=UAS-MECP2.#.GW.*}attP40***,** where # represents the variant and * represents
222 integrant line number (Supplemental Data 1).
223
224 **Crossing scheme**
225 Experimenters were double blinded to genotype throughout. Homozygous *UAS-MECP2* males
226 and a control *attP40* line were crossed to *A9-GAL4* virgins (ratio 4 males : 12 females), and
227 maintained at room temperature (~21 °C ) for 72 hours. Crosses were then transferred into fresh
228 'assay' vials, and transferred each 24 hrs each for three days, generating three 'assay' vials per

229 cross. After removal of adults from each vial, vials were placed into a 29 °C incubator (70%
230 humidity). Three days after eclosion, adult flies were sorted by sex and placed in pure
231 isopropanol at -20 °C. All progeny flies for comparison were tested in a single batch.
232
233 **Wing imaging**
234 Experimenters were double blinded to genotype throughout. Flies were removed from
235 isopropanol, dried on paper towels, and 10-25 left wings were removed per genotype per assay
236 vial (one wing per fly). Wings were mounted on microscope slides in Canadian Balsam Fir
237 (1.01691.0025, CAS-No: 8007-47-4, Sigma Aldrich, MA, USA), coverslipped and sealed with
238 nail polish. Females have larger wings and the X-linked *A9-GAL4* driver is expressed at higher
239 levels in males, due to X-chromosome male-hyperactivation. Thus, it is important to analyze
240 males and females separately. While the impact of MECP2 variants in the wing was similar
241 between males and females, the phenotype was substantially stronger in males due to the higher
242 GAL4 levels; hence, higher MECP2 levels. To simplify analysis, we therefore only fully
243 analyzed male wings. Slides were compressed while drying for 24 hrs. Mounted wings were
244 scanned using a Panoramic Midi II digital slide scanner (3DHISTECH, Budapest, Hungary).
245 Scanned fly wing images were cropped at 15x zoom using CaseViewer (3DHISTECH,
246 Budapest,Hungary). Images were imported into Imaris v10.0 software (Bitplane, MA, USA) for
247 measurement of wing vein area per wing area, using Labkit machine learning and Fiji software
248 (University of Wisconsin-Madison, USA). In Labkit, we developed
249 "BIGSMOOTHCLASSYBOI", a machine learning algorithm to automate measurement of wing
250 vein area for calculation of wing vein area/wing area (details provided in Supplemental Methods
251 1).

252

253 **Statistical analysis of variant effects**

254 Yeast growth constants (k) and fly relative wing vein area data were analyzed using methods
255 similar to Post et al. (Post et al. 2020). Briefly, linear mixed-effects models were fit to each data
256 set using the *lmerTest* R package (Kuznetsova et al. 2017) to estimate the phenotypic effects of
257 each variant compared to the *MECP2-ref* constructs, treating experimental batches as random
258 effects (for R scripts see Supplemental Methods 2 and 3). For visualization, values were
259 standardized to the range [0-1] where 0 represents the mean phenotype measured for an empty
260 vector, and 1 represents the mean phenotype with the *MECP2-ref* construct. Four biological
261 replicates, each with three technical replicates were performed for yeast variant growth assays,
262 while for *Drosophila* wing assays 10-25 wings, each from a different animal were imaged per
263 genotype.

264

265 **RESULTS**

266 ***Selection of variants***

267 We selected benign and pathogenic variants with clear clinical classifications to calibrate our
268 functional assays, and nine test (ASD) variants (Figure 1, Supplemental Data 1). We focused on
269 ClinVar variants with "pathogenic", "likely_pathogenic", "benign" and "likely_benign" clinical
270 interpretation as calibration variants. Priority was given to those with either "reviewed by expert
271 panel" or "criteria provided, multiple submitters" review status. A few exceptions were made.
272 D121E, a single-submitter benign variant, and T148A, originally classified as benign, but now
273 listed as conflicting were selected because there were no other benign variants in the MBD that
274 matched the aforementioned criteria. When selecting pathogenic variants, in addition to using

275 review status as a criterion, we also prioritized the ones with "Rett syndrome" condition
276 annotation as well as the ones that have been frequently observed in Rett patients (Good et al.
277 2021). In total, we selected 37 calibration variants, 10 benign and 27 pathogenic. We selected
278 ASD MECP2 variants from VariCarta as test variants as long as they did not have a clear clinical
279 interpretation in ClinVar, for the total of 9 test (ASD) variants. Since the time of our initial
280 selection, six test (ASD) variants have been given updated classifications in ClinVar: P152L,
281 P217L and E282G becoming pathogenic/ likely pathogenic, and G195S, P376S and P388S
282 becoming benign (Figure 1 displays the initial classifications).
283
284 ***MECP2 produces a slow growth phenotype in yeast***
285 *MECP2-ref* was cloned into a high-copy 2-micron plasmid designed to give controlled
286 expression in response to addition of estradiol. Using an anti-MECP2 antibody we monitored
287 MECP2 protein levels by Western blot in response to increasing estradiol (Figure 2A). In the no-
288 estradiol condition we detected low levels of MECP2 protein, which increased with increasing
289 estradiol and then saturated at ~10 nM. Next, we measured the growth rate of WT yeast
290 containing either the *MECP2-ref* plasmid or an empty vector control in response to estradiol
291 addition (Figure 2B). Compared to empty vector which had little effect in response to increasing
292 estradiol, yeast containing MECP2 showed a dose-dependent decrease in exponential growth
293 rate. We compared this to another vector designed for strong overexpression utilizing the
294 *Gal1/10* promoter in a 2-micron vector and observed an even greater decrease in growth rate in
295 the presence of MECP2 (Figure 2C). Thus, expression of MECP2 reduced the fitness of WT
296 yeast in a dose-dependent manner.
297

298 ***MECP2 expression affects DNA-related processes in yeast***

299 To understand how MECP2 might be functioning in yeast and if this is related to the normal
300 function of MECP2 we employed a genetic interaction mapping approach we previously
301 developed to study the function of human genes in yeast, called Sentinel Interaction Mapping
302 (SIM) (Young et al. 2020). For SIM we express the human gene of interest in a collection of
303 nearly 4,800 yeast deletion mutants and systematically identify genetic interactions, which
304 indicate functional associations between the human gene and yeast cellular pathways. Hence,
305 these genetic interactions will inform us on the function of the human gene in yeast and if this is
306 relevant to its function in humans. We performed a SIM screen with *MECP2-ref* in which
307 MECP2, under control of the estradiol responsive promoter in the 2-micron vector, was
308 expressed in ~ 4,800 different yeast deletion mutant strains in high-density arrays (see Methods
309 for details). Colony sizes were scored using Balony software and genetic interactions were
310 identified by comparing control arrays containing no estradiol (uninduced) to experimental
311 arrays containing 10 nM estradiol (induced). We chose 10 nM estradiol because MECP2 protein
312 expression saturated at this concentration and the effect on growth was not too severe, which
313 would otherwise hinder identification of genetic interactions.

314

315 The SIM screen identified 123 aggravating genetic interactions in 3/3 biological replicates
316 (Supplemental Data 2). We examined functional enrichment for these interactions using Gene
317 Ontology (GO) analysis (Figure 3A; also see Supplemental Data 3 for gene lists). This revealed a
318 network of interconnected functions related to DNA and chromosome stability, with the most
319 significant enrichment being for the terms “Cellular response to stress” (30 genes) and “DNA
320 damage response” (24 genes). Functions related to DNA binding (27 genes), cell cycle (21

321 genes), Golgi (8 genes) and nitrogen compound utilization (17 genes) were also enriched for.
322 The large enrichment for DNA-related functions was consistent with MECP2 being a DNA
323 binding protein with roles in transcriptional repression and chromatin organization. We focused
324 on a subset of interactions from GO terms most relevant to MECP2 function. Shown in Figure
325 3B is the effect on growth of the individual mutants from the screen upon MECP2 induction for
326 the GO terms "Chromatin organization", "DNA binding" and "DNA damage response". Because
327 these are aggravating interactions, MECP2 induction (10 nM estradiol) resulted in decreased
328 growth rate of the mutants relative to no induction (0 nM estradiol). Growth was normalized to
329 account for the effect of MECP2 induction on WT yeast growth.
330
331 Looking more closely at these genes, we identified five out of the ten members of the *RAD52*
332 epistasis group, *RAD50/51/52/54* and *XRS2* (*RAD55/57/59*, *RDH54* and *MRE11* were not
333 identified) (Figure 3B). Mutants in this group are defective in the repair of DNA damage,
334 maintenance of telomere length and meiotic and mitotic recombination (Symington 2002). We
335 also identified three out of four of the subunits of the highly conserved MRX endo/exonuclease
336 complex, which functions in repair of DNA double strand breaks, detection of damaged DNA,
337 DNA damage checkpoint activation, telomerase recruitment and suppression of chromosomal
338 defects (Syed and Tainer 2018). We identified Rad50, Xrs2 and Sae2, but not *MRE11* in our
339 screen (Figure 3B). *RAD50* and *XRS2* were among the strongest interactions such that MECP2
340 expression reduced growth of the *rad50*Δ and *xrs2*Δ mutants to almost undetectable levels.
341
342 We also identified both subunits of the SBF transcription factor complex, Swi4 and Swi6. Swi6
343 is also a component of the MBF complex (MBF comprises Swi6 and Mbp1), which along with

344 SBF functions to regulate transcription of the G1/S gene cluster as well as transcription of genes
345 involved in DNA synthesis and repair (Bähler 2005). *swi6*Δ cells grow slowly, have a delayed
346 G1/S transition and are sensitive to DNA damaging agents. Expression of MECP2 in the *swi6*Δ
347 mutant severely reduced growth indicating a strong interaction. Additionally, we identified a
348 strong interaction with the cyclin-dependent kinase *PHO85*, which regulates many cellular
349 processes in response to stress and also plays an important role in G1/S transition via interaction
350 with various G1 cyclins (Jiménez et al. 2013). Δ*pho85* cells grow slowly, have increased mitotic
351 chromosome loss and shortened telomeres. Taken together, these strong aggravating interactions
352 with genes with central functions in DNA synthesis and repair, chromatin organization and G1/S
353 cell cycle progression suggested MECP2 expression severely antagonized these processes which
354 resulted in reduced fitness.
355
356 ***Assessment of MECP2 variants in yeast***
357 We decided to simply exploit the robust slow growth phenotype observed upon MECP2
358 expression in WT yeast to determine the effects of MECP2 variants, anticipating variants that
359 interfered with MECP2 function would no longer reduce growth. We measured yeast growth in
360 liquid culture for all 46 variants using the galactose-inducible 2-micron vector, because this
361 vector produced the largest growth defect. We calculated exponential growth rates for WT yeast
362 expressing MECP2 variants and using a linear mixed-effects model estimated the effects of the
363 variants on MECP2 function (raw data is provided in Supplemental Data 4). Shown in Figure 4A
364 is the model's estimates of MECP2 function, arranged by variant amino acid position. Values
365 were standardized to the range [0-1] where 0 represents the mean phenotype measured for an
366 empty vector, and 1 represents the mean phenotype with the *MECP2-ref* construct. Hence,

367 variants with values near to 1 functioned similarly to MECP2-ref, whereas values greater or less
368 than 1 indicated increased or decreased function, respectively (error is plotted as 95% confidence
369 intervals).
370
371 Benign calibration variants had little effect on function as expected across all MECP2 domains.
372 The one exception was the D121E variant which was nearly complete LoF, for which we have
373 additional supporting evidence in fly leading to reclassification of this variant as pathogenic (see
374 below). For the MBD domain, all seven pathogenic calibration variants were complete or near-
375 complete LoF (we define a variant is complete LoF when its 95% confidence interval overlaps
376 with 0). This supported that our assay was disease-relevant for variants in the MBD. L100V,
377 R106W, R133C, and T158M have been previously reported to have reduced DNA binding *in*
378 *vitro* and *in vivo* (Tillotson and Bird 2020), suggesting our assay reported on this function of the
379 MBD. Residue R133 is part of the DNA interface and interacts directly with guanine of the
380 mCpG island, and T158 is part of the Asx-ST motif that interacts with the DNA backbone
381 (Tillotson and Bird 2020). The two test (ASD) variants in this domain, R91W and P152L, were
382 found to have decreased function, although not as severe as the calibrating pathogenics. In
383 contrast, calibrating pathogenics outside the MBD generally did not show decreased function.
384 This indicated the yeast assay could not reliably detect altered function for variants outside the
385 MBD.
386
387 ***Protein level of variants in yeast***
388 We measured protein levels for all variants in the MBD to determine if decreased stability/
389 increased turnover might be a factor in our assessment of function. We also included additional

390 non-MBD calibrating benigns from the TRD (T228S) and the CTD (S356G) for comparison; and
391 P388S because this variant showed the most reduced function of all non-MBD variants. MECP-2
392 protein levels from yeast extracts were measured on Western blots and normalized to MECP2-ref
393 (Figure 4B and Supplemental Figure 1). For the MBD, 8 out of 13 MBD variants had reduced
394 levels relative to MECP2-ref, while 5 were not significantly different from MECP2-ref. Variants
395 with decreased protein levels ranged from ~65% (T148A) to ~37% (R106W) of MECP2-ref. The
396 two calibrating benigns outside the MBD, T228S and S356G, did not show decreased protein
397 levels, whereas the test (ASD) variant P388S had substantially reduced protein levels (~ 25% of
398 MECP2-ref).
399
400 Comparing protein levels to function of variants there appeared to be little correlation. Some
401 variants had normal protein levels yet were non-functional (L100V, P101S, D121E, R133C).
402 Other variants showed both decreased protein levels and decreased function (R106W, T158M,
403 G163W, P388S). This suggested in some cases the variant affected MECP2 DNA binding
404 directly leading to decreased function (e.g., R133C), whereas in other cases decreased function
405 might also be a result of destabilization/ increased turnover (e.g., R106W). To investigate this in
406 more detail we looked to variants outside the MBD, because these should not directly affect
407 DNA binding. P388S was the only variant outside the MBD that showed moderate LoF (~ 50%;
408 Figure 3A) and we found it to have greatly reduced protein levels, whereas a variant in the same
409 domain, S356G, was functional and had normal protein levels. The modest decrease in function
410 of P388S relative to its low protein levels, suggested our functional assay was relatively
411 insensitive to destabilization. The T148A variant, which had reduced protein levels (~65% of
412 MECP2-ref), but was completely functional in the assay, further supported this conclusion.

413 Overall, these data suggested the yeast functional assay primarily reported on the intrinsic DNA
414 binding ability of the MECP2 MBD.
415
416 ***Using a fly wing vein assay for assessing MECP2 variant function***
417 Expression of *MECP2* in *Drosophila* tissues has a wide range of phenotypes (Cukier et al. 2008;
418 Vonhoff et al. 2012; Williams, White, et al. 2016; Williams, Mehler, et al. 2016). From these
419 reports, we chose to assess MECP2 variants in developing wing tissues. This was because (1) the
420 reported ectopic wing vein phenotype could be exploited here to provide a quantitative readout
421 of MECP2 variant protein function, and (2) *MECP2* was shown to genetically interact with
422 known MECP2 co-repressor complexes in the context of this specific phenotype (Cukier et al.
423 2008), suggesting the wing vein phenotype was relevant to MECP2 function in humans. These
424 provided strong precedence for using this wing vein assay for assessing the function of ASD
425 variants in MECP2.
426
427 We integrated *UAS-MECP2-ref* into the *attP40* locus on the *pGW.HA.attB* transgenic vector
428 backbone to control for genome position effect and copy number (Bischof et al. 2007), to reduce
429 variability in expression levels between integrants. In pilot experiments we tested a range of
430 conditions including wing imaginal disc *GAL4* drivers, incubation temperatures and sex of
431 progeny (as females have larger wings). We found that the ideal set of variables to produce a
432 robust ectopic wing vein phenotype were the *A9-GAL4* driver in males (X-chromosome
433 hyperactivation in male flies results in higher GAL4/UAS activity) raised at 29 $^{o}$C (Figure 5,
434 arrows). We also noted *MECP2-ref* expression resulted in smaller wings (Figure 5). Thus, we
435 could proceed with assessing the effects of variants using this assay.

436

437 ***Assessment of 25 MECP2 variants using the wing vein assay***

438 In total 25 transgenic lines were generated, including eight calibrating benign, eight calibrating
439 pathogenic and nine test (ASD) variants. For all transgenic lines we passaged mating adults
440 through three consecutive 'assay' vials. Adult progeny were then collected 3 days post-eclosion
441 from each assay vial, and a single wing from a minimum of 10 adult male progeny per assay vial
442 was removed and slide-mounted, for a total of 30 wings per variant. Mounted wings were
443 scanned and total wing vein area / wing area was analyzed using a Labkit machine learning
444 algorithm that semi-automated the quantitation of wing vein area (see Methods).

445

446 Next, we examined wing vein phenotypes induced by expression of all 25 MECP2 variants, with
447 *attP40* and *MECP2-ref* controls in parallel. Representative images for controls, selected
448 calibrating benign and pathogenic variants and all test (ASD) variants are shown in Figure 5
449 (also see Supplemental Figures 2 and 3 for representative images of all MECP2 variants and the
450 masked area that was considered to contain vein tissue). Benign calibration variants all showed
451 increased ectopic wing veins (T203M and T228S are shown) whereas calibrating pathogenics
452 showed very little (L100V and T158M are shown), and test (ASD) variants had a range of
453 outcomes (Figure 5). For example, P376S showed increased ectopic wing veins similar to
454 *MECP2-ref* whereas P152L had few extra wing veins.

455

456 To quantify this phenotype, we trained two machine learning algorithms to quantify (1) the total
457 area of the wing vein region and (2) the total area of the wing (see Supplemental Data 5 for
458 details). Then using a linear mixed effects model these two values were used to calculate the

459 estimated effect of variants relative to *MECP2-ref* and were normalized to *MECP2-ref* (at 1) and
460 *attp40* (at 0) (Figure 6, error bars are 95 % confidence intervals). All benign calibration variants
461 functioned similar to *MECP2-ref*, except for D121E. This variant was classified in ClinVar as
462 benign by a single contributor, but we find both yeast and fly assays characterized it as a strong
463 LoF, hence we predict D121E is likely pathogenic. All pathogenic calibration variants showed
464 varying degrees of LoF, indicating the wing vein assay reported on disease relevant functions for
465 MECP2. Most were strong LoF variants, except for P225R, which had reduced function but not a
466 complete LoF. This successful calibration of the assay indicated clinically pathogenic and benign
467 variants can be correctly classified in the fly model. We were particularly confident for variants
468 in the MBD and TRD domains, because we tested multiple calibrating pathogenics in these
469 domains, and both DNA and co-repressor interactions through these domains are validated in this
470 assay. In the same experimental batch as the calibrating benign and pathogenic variants
471 (controlling for food, temperature and humidity), we determined the wing vein phenotype for all
472 nine test (ASD) variants. We found that both MBD variants R91W and P152L were LoF. The
473 TRD variants P217L and E282G exhibited a partial LoF with data distributed similarly to the
474 TRD pathogenic variant P225R. Finally, the Interdomain (G195S, A202G) and CTD variants
475 (P376S, P388S and S411R) all exhibited normal function, similar to the calibrating benigns.
476 Thus, we conclude that only test (ASD) variants in the MBD and TRD domains were LoF.
477
478 Finally, we compared yeast and fly assay results for MBD variants only, because the yeast assay
479 could only reliably measure MBD variants. We observed remarkable similarity in results
480 between the two assays. Of particular interest was that both test (ASD) variants R91W and
481 P152L appeared more functional in both yeast and fly assays than the pathogenic calibration

482 variants. This suggested ASD variants may retain more DNA binding capacity than Rett variants,
483 given these assays likely reported on the intrinsic ability of MECP2 to bind DNA.
484
485 **DISCUSSION**
486 ***Clinical classification of variants***
487 Using our assays calibrated with variants classified in ClinVar as pathogenic and benign, we are
488 able to provide functional assessments for nine test (ASD) variants, five of which have been
489 found in cases of ASD without Rett (underlined): R91W, P152L, G195S, A202G, P217L,
490 E282G, P376S, P388S, S411R (Figure 1). We found that R91W and P152L were LoF variants
491 (yeast and fly) and we classify these as likely pathogenic. Our classification for P152L agrees
492 with the updated pathogenic ClinVar classification and we re-classify R91W from a VUS in
493 ClinVar. G195S had a modest gain of function (fly), hence we classify it as likely benign. Our
494 likely pathogenic classification for G195S agrees with the updated benign ClinVar classification.
495 A202G was found to be functional (fly). The ClinVar classification for this variant is conflicting
496 (one benign and one VUS report) and we propose this variant be classified as likely benign.
497 P217L and E282G showed moderately reduced function (fly) consistent with their updated likely
498 pathogenic ClinVar classifications. P376S, P388S and S411R were found to be functionally
499 normal (fly). For P376S and P388S this is consistent with their updated benign classifications in
500 ClinVar. However, since P388S appeared to be a destabilized protein in yeast we suggest P388S
501 is worthy of further examination. We classify S411R as likely benign providing the first
502 classification for this variant. Importantly, we provide functional evidence to classify two
503 variants found in ASD but not Rett as likely pathogenic (R91W, E282G), suggesting certain
504 mutations in MECP2 may cause ASD while others will cause Rett. Further, our data suggest

505 variants found in ASD but not Rett may be less severe than Rett causing mutations, since the
506 ASD-only variants we tested were more functional than Rett causing variants.
507
508 Finally, we provide evidence for reclassification of two variants, D121E and T148A, currently
509 classified in ClinVar as benign and conflicting, respectively. D121E was LoF in both yeast and
510 *Drosophila* assays, hence we propose D121E be reclassified as likely pathogenic. Interestingly,
511 our data are consistent with *in vitro* studies showing a ~7-fold reduction in the DNA binding
512 capacity of the D121E variant (Free et al. 2001). This variant is neither in VariCarta nor
513 RettBASE and it has one report in ClinVar, but this report lacks a description for how a benign
514 classification was made. Interestingly, the computational predictors SIFT, PolyPhen and CADD
515 all predict this variant is likely to be LoF (Supplemental Data 1), supporting our likely
516 pathogenic classification. For T148A, the current ClinVar classification is conflicting. We find
517 this variant to be functional (yeast), but to have modestly decreased protein levels (~65% of
518 MECP2-ref), suggesting it may have reduced stability. SIFT, PolyPhen and CADD all predict
519 this variant to be damaging. We propose T148A be reclassified as likely benign, but suggest
520 further characterization is warranted.
521
522 ***Calibrating functional assays by protein domain***
523 Often proteins contain multiple domains which contribute distinct functions to the protein. Our
524 results indicate that when developing functional assays for human proteins in evolutionarily
525 distant model organisms it is important to calibrate assays for each domain. This can be achieved
526 through inclusion of calibration variants with known clinical/biochemical designations covering
527 each domain. MEPC2 is a multi-domain protein and is largely unstructured outside the MBD

528 domain (Ghosh et al. 2010). We initially focused on identifying calibrating variants in the MBD
529 and TRD domains, as these domains harbour many of the clinically relevant variants.
530
531 The yeast assay only calibrated for the MBD and failed to calibrate for all other domains,
532 indicating we could only assess functional effects of variants found within the MBD. A likely
533 explanation is that the MECP2 MBD binds DNA in yeast without the need of accessory factors.
534 Indeed, Brown *et al.*, show this is likely to be the case (Brown et al. 2025 Mar 18). The TRD
535 mediates interactions with co-repressor complexes, including Sin3A, N-Cor and REST, and Rett-
536 causing mutations disrupt these interactions (Lyst et al. 2013). It is likely the assay failed to
537 calibrate for TRD variants because these complexes are either not present in yeast (N-Cor and
538 REST), or the TRD did not interact with the yeast ortholog (Sin3A/HDAC). The results of the
539 MECP2 SIM screen also provided valuable insight into MECP2's function in yeast. The strong
540 aggravating genetic interactions we observed with genes involved in DNA damage response and
541 DNA repair pathways (e.g., *RAD50*) suggest MECP2 expression either directly or indirectly
542 results in DNA damage. These effects of MECP2 likely disrupted the cell cycle (supported by
543 the interactions with cell cycle genes, e.g., *PHO85*) leading to overall decreased cell growth.
544 Since variants in the MBD known to disrupt DNA binding failed to inhibit growth, this further
545 suggested DNA binding by MECP2 contributed to defects in DNA and/or chromatin.
546
547 *Drosophila* was successful in stratifying pathogenic and benign calibration variants in both the
548 MBD and TRD domains, indicating we can make high confidence predictions about test ASD
549 variants located in these domains. For variants in the MBD, it is likely these disrupt DNA
550 binding, although DNA binding by MECP2 has yet to be demonstrated in *Drosophila*. For the

551 TRD, our data suggest MECP2 is able to interact with *Drosophila* orthologs of co-repressor
552 complexes. First, R306C prevents interaction with co-repressors and was complete LoF in our
553 assay (Lyst et al. 2013). Second, co-repressor complex mutants suppress phenotypes resulting
554 from MECP2 over-expression in the *Drosophila* wing (Cukier et al. 2008). For example,
555 mutation of the Polycomb group co-repressor ortholog of Asxl1, *Asx*, prevents ectopic wing vein
556 growth resulting from MECP2 expression (Cukier et al. 2008). For the Interdomain and CTD
557 domain, testing additional pathogenic variants in these domains would increase confidence in our
558 predictions for test (ASD) variants within these domains. Thus, when developing functional
559 assays in surrogate model systems with considerable evolutionary distance from humans, it is
560 important to consider calibrating assays for each domain before making conclusions about the
561 effects of test variants.
562
563 ***MECP2 protein stability***
564 The stability of a handful of MECP2 variants has been studied both using *in vitro* assays and *in*
565 *vivo* mouse models (Kucukkal et al. 2015; Yang et al. 2016; Sperlazza et al. 2017; Tillotson and
566 Bird 2020). We were able to compare seven variants located in the MBD between our yeast
567 results and these studies (Supplemental Table 1). R106W, P152R and T158M are all destabilized
568 in mouse models and *in vitro* systems, and based on protein levels in yeast were predicted to be
569 also destabilized in yeast also. R133C is found to be stable in *in vitro* systems and is predicted to
570 be stable in yeast, but is destabilized in mouse. L100V and P101S are destabilized *in vitro*, but
571 are predicted to be stable in yeast. R133H is stable *in vitro*, but is predicted to be destabilized in
572 yeast. Hence, the discrepancies between these data emphasize the value of comparing variant
573 function across multiple species and assay systems. MECP2 turnover in cells is regulated by

574 ubiquitylation by the E3 ligase RNF4 (Wang 2014), indicating it may be an *in vivo*-specific
575 modifier of variant stability. Interestingly, we identified the yeast orthologs of RNF4, *SLX5* and
576 *SLX8*, as aggravating genetic interactions in our SIM screen (Figure 3B), suggesting MECP2
577 levels may also be regulated by this E3 ligase in yeast. Thus, regulated turnover *in vivo* is likely
578 an important factor contributing to MECP2 variant function and may vary across assay systems.
579 Interaction of MECP2 with DNA and co-repressors also influences MECP2 intrinsic stability
580 (Ghosh et al. 2010), hence differences in these interactions could be another factor contributing
581 to differences in MECP2 variant function/stability between assay systems.
582
583 ***MECP2 and DNA methylation***
584 It is noteworthy that all pathogenic calibration variants in the MBD were LoF in our functional
585 assays despite there being no, or extremely low levels of DNA cytosine methylation in yeast and
586 *Drosophila*, respectively. Our data correlate well with Brown *et al.* (Brown et al. 2025 Mar 18),
587 showing that MECP2 binds the unmethylated yeast genome and mediates widespread
588 transcriptional suppression. This raises the possibility that ASD and Rett MECP2 variants may
589 not be specifically deficient in their ability to bind methylated DNA, but may be generally
590 deficient in binding to unmethylated DNA and/or chromatin. It is challenging to specify
591 differential impacts of specific Rett variants on methyl versus non-methyl DNA binding in
592 models where DNA methylation is present. We propose this may have obscured the impact that
593 pathogenic variants have on non-methylated DNA binding and its importance in healthy and
594 disease states, and we propose that the yeast and fly models offer valuable platforms to further
595 examine these mechanisms.
596

597 **DATA AVAILABILITY STATEMENT**

598 Strains and plasmids are available upon request. The authors affirm that all data necessary for
599 confirming the conclusions of the article are present within the article, figures, tables and
600 supplemental data files.

601

602 **ACKNOWLEDGEMENTS**

603 We thank Dr. Janel Kopp, UBC for access to the Panoramic Midi II digital slide scanner. Susan
604 Lindquist for the generous gift of the *pAG426GAL-ccdB* vector. Stocks obtained from the
605 Bloomington *Drosophila* Stock Center (NIH P40OD018537) were used in this study. We thank
606 *Drosophila* Genomics Resource Center, supported by NIH grant 2P40OD010949 for the *esc*
607 cDNA. We used FlyBase (releases 2020 through 2024) for general information on genes,
608 phenotypes and stocks. We would like to thank Gino Laberge at Genome ProLab for the kind
609 gift of balancer stocks and also their transgenic services (Genome ProLab Inc, Quebec, Canada).
610 We thank Libby Natola and Guillaume Poirier-Morency (Pavlidis Lab) for contributions to the
611 variant annotation pipeline. This work was funded by an operating grant from The Simons
612 Foundation Autism Research Initiative (2021 Genomics of ASD: Pathway to Genetic Therapies:
613 AWD-021951. SIMOFOUN 2021).

614

615 **REFERENCES**

616 Amir RE, Van den Veyver IB, Schultz R, Malicki DM, Tran CQ, Dahle EJ, Philippi A, Timar L,
617 Percy AK, Motil KJ, et al. 2000. Influence of mutation type and X chromosome inactivation on
618 Rett syndrome phenotypes. Ann Neurol. 47(5):670–679.

619 Amir RE, Van den Veyver IB, Wan M, Tran CQ, Francke U, Zoghbi HY. 1999. Rett syndrome
620 is caused by mutations in X-linked MECP2, encoding methyl-CpG-binding protein 2. Nat Genet.
621 23(2):185–188. doi:10.1038/13810.

622 Ananth A, Fu C, Neul JL, Benke T, Marsh E, Suter B, Ferdinandsen K, Skinner SA, Annese F,
623 Percy AK. 2024. MECP2 Variants in Males: More Common than Previously Appreciated.
624 Pediatr Neurol. 161:263–267. doi:10.1016/j.pediatrneurol.2024.09.022.

625 Bähler J. 2005. Cell-Cycle Control of Gene Expression in Budding and Fission Yeast. Annu Rev
626 Genet. 39(Volume 39, 2005):69–94. doi:10.1146/annurev.genet.39.110304.095808.

627 Ballestar E, Yusufzai TM, Wolffe AP. 2000. Effects of Rett Syndrome Mutations of the Methyl-
628 CpG Binding Domain of the Transcriptional Repressor MeCP2 on Selectivity for Association
629 with Methylated DNA. Biochemistry. 39(24):7100–7106. doi:10.1021/bi0001271.

630 Belmadani M, Jacobson M, Holmes N, Phan M, Nguyen T, Pavlidis P, Rogic S. 2019. VariCarta:
631 A Comprehensive Database of Harmonized Genomic Variants Found in Autism Spectrum
632 Disorder Sequencing Studies. Autism Res Off J Int Soc Autism Res. 12(12):1728–1736.
633 doi:10.1002/aur.2236.

634 Bischof J, Maeda RK, Hediger M, Karch F, Basler K. 2007. An optimized transgenesis system
635 for Drosophila using germ-line-specific phiC31 integrases. Proc Natl Acad Sci U S A.
636 104(9):3312–3317. doi:10.1073/pnas.0611511104.

637 Brnich SE, Abou Tayoun AN, Couch FJ, Cutting GR, Greenblatt MS, Heinen CD, Kanavy DM,
638 Luo X, McNulty SM, Starita LM, et al. 2019. Recommendations for application of the functional
639 evidence PS3/BS3 criterion using the ACMG/AMP sequence variant interpretation framework.
640 Genome Med. 12:3. doi:10.1186/s13073-019-0690-2.

641 Brown JAR, Ling MYM, Ausió J, Howe LJ. 2025 Mar 18. Human MeCP2 binds to promoters
642 and inhibits transcription in an unmethylated yeast genome. Genetics.:iyaf043.
643 doi:10.1093/genetics/iyaf043.

644 Buitrago D, Labrador M, Arcon JP, Lema R, Flores O, Esteve-Codina A, Blanc J, Villegas N,
645 Bellido D, Gut M, et al. 2021. Impact of DNA methylation on 3D genome structure. Nat
646 Commun. 12(1):3243. doi:10.1038/s41467-021-23142-8.

647 Chahrour M, Zoghbi HY. 2007. The Story of Rett Syndrome: From Clinic to Neurobiology.
648 Neuron. 56(3):422–437. doi:10.1016/j.neuron.2007.10.001.

649 Cheng T-L, Wang Z, Liao Q, Zhu Y, Zhou W-H, Xu W, Qiu Z. 2014. MeCP2 suppresses nuclear
650 microRNA processing and dendritic growth by regulating the DGCR8/Drosha complex. Dev
651 Cell. 28(5):547–560. doi:10.1016/j.devcel.2014.01.032.

652 Cukier HN, Perez AM, Collins AL, Zhou Z, Zoghbi HY, Botas J. 2008. Genetic Modifiers of
653 MeCP2 Function in Drosophila. PLoS Genet. 4(9):e1000179. doi:10.1371/journal.pgen.1000179.

654 Ehrhart F, Jacobsen A, Rigau M, Bosio M, Kaliyaperumal R, Laros JFJ, Willighagen EL,
655 Valencia A, Roos M, Capella-Gutierrez S, et al. 2021. A catalogue of 863 Rett-syndrome-
656 causing MECP2 mutations and lessons learned from data integration. Sci Data. 8(1):10.
657 doi:10.1038/s41597-020-00794-7.

658 Free A, Wakefield RID, Smith BO, Dryden DTF, Barlow PN, Bird AP. 2001. DNA Recognition
659 by the Methyl-CpG Binding Domain of MeCP2 *. J Biol Chem. 276(5):3353–3360.
660 doi:10.1074/jbc.M007224200.

661 Ganguly P, Madonsela L, Chao JT, Loewen CJR, O'Connor TP, Verheyen EM, Allan DW.
662 2021. A scalable Drosophila assay for clinical interpretation of human PTEN variants in
663 suppression of PI3K/AKT induced cellular proliferation. PLoS Genet. 17(9):e1009774.
664 doi:10.1371/journal.pgen.1009774.

665 Georgel PT, Horowitz-Scherer RA, Adkins N, Woodcock CL, Wade PA, Hansen JC. 2003.
666 Chromatin compaction by human MeCP2. Assembly of novel secondary chromatin structures in
667 the absence of DNA methylation. J Biol Chem. 278(34):32181–32188.
668 doi:10.1074/jbc.M305308200.

669 Ghosh RP, Nikitina T, Horowitz-Scherer RA, Gierasch LM, Uversky VN, Hite K, Hansen JC,
670 Woodcock CL. 2010. Unique physical properties and interactions of the domains of methylated
671 DNA binding protein 2. Biochemistry. 49(20):4395–4410. doi:10.1021/bi9019753.

672 Good KV, Vincent JB, Ausió J. 2021. MeCP2: The Genetic Driver of Rett Syndrome
673 Epigenetics. Front Genet. 12:620859. doi:10.3389/fgene.2021.620859.

674 Guo H, Wang T, Wu H, Long M, Coe BP, Li H, Xun G, Ou J, Chen B, Duan G, et al. 2018.
675 Inherited and multiple de novo mutations in autism/developmental delay risk genes suggest a
676 multifactorial model. Mol Autism. 9(1):64. doi:10.1186/s13229-018-0247-z.

677 Hansen JC, Ghosh RP, Woodcock CL. 2010. Binding of the Rett syndrome protein, MeCP2, to
678 methylated and unmethylated DNA and chromatin. IUBMB Life. 62(10):732–738.
679 doi:10.1002/iub.386.

680 Harikrishnan KN, Chow MZ, Baker EK, Pal S, Bassal S, Brasacchio D, Wang L, Craig JM,
681 Jones PL, Sif S, et al. 2005. Brahma links the SWI/SNF chromatin-remodeling complex with
682 MeCP2-dependent transcriptional silencing. Nat Genet. 37(3):254–264. doi:10.1038/ng1516.

683 Her Y, Pascual DM, Goldstone-Joubert Z, Marcogliese PC. 2024. Variant functional assessment
684 in Drosophila by overexpression: what can we learn? Genome. 67(6):158–167. doi:10.1139/gen-
685 2023-0135.

686 Jiménez J, Ricco N, Grijota-Martínez C, Fadó R, Clotet J. 2013. Redundancy or specificity? The
687 role of the CDK Pho85 in cell cycle control. Int J Biochem Mol Biol. 4(3):140–149.

688 Jones PL, Veenstra GJ, Wade PA, Vermaak D, Kass SU, Landsberger N, Strouboulis J, Wolffe
689 AP. 1998. Methylated DNA and MeCP2 recruit histone deacetylase to repress transcription. Nat
690 Genet. 19(2):187–191. doi:10.1038/561.

691 Kucukkal TG, Yang Y, Uvarov O, Cao W, Alexov E. 2015. Impact of Rett Syndrome Mutations
692 on MeCP2 MBD Stability. Biochemistry. 54(41):6357–6368. doi:10.1021/acs.biochem.5b00790.

693 Kuznetsova A, Brockhoff PB, Christensen RHB. 2017. lmerTest Package: Tests in Linear Mixed
694 Effects Models. J Stat Softw. 82:1–26. doi:10.18637/jss.v082.i13.

695 Landrum MJ, Lee JM, Benson M, Brown GR, Chao C, Chitipiralla S, Gu B, Hart J, Hoffman D,
696 Jang W, et al. 2018. ClinVar: improving access to variant interpretations and supporting
697 evidence. Nucleic Acids Res. 46(D1):D1062–D1067. doi:10.1093/nar/gkx1153.

698 Leblond CS, Le T-L, Malesys S, Cliquet F, Tabet A-C, Delorme R, Rolland T, Bourgeron T.
699 2021. Operative list of genes associated with autism and neurodevelopmental disorders based on
700 database review. Mol Cell Neurosci. 113:103623. doi:10.1016/j.mcn.2021.103623.

701 Lewis JD, Meehan RR, Henzel WJ, Maurer-Fogy I, Jeppesen P, Klein F, Bird A. 1992.
702 Purification, sequence, and cellular localization of a novel chromosomal protein that binds to
703 Methylated DNA. Cell. 69(6):905–914. doi:10.1016/0092-8674(92)90610-O.

704 Lunyak VV, Burgess R, Prefontaine GG, Nelson C, Sze S-H, Chenoweth J, Schwartz P, Pevzner
705 PA, Glass C, Mandel G, et al. 2002. Corepressor-Dependent Silencing of Chromosomal Regions
706 Encoding Neuronal Genes. Science. 298(5599):1747–1752. doi:10.1126/science.1076469.

707 Lyko F, Ramsahoye BH, Jaenisch R. 2000. DNA methylation in Drosophila melanogaster.
708 Nature. 408(6812):538–540. doi:10.1038/35046205.

709 Lyst MJ, Ekiert R, Ebert DH, Merusi C, Nowak J, Selfridge J, Guy J, Kastan NR, Robinson ND,
710 de Lima Alves F, et al. 2013. Rett syndrome mutations abolish the interaction of MeCP2 with the
711 NCoR/SMRT co-repressor. Nat Neurosci. 16(7):898–902. doi:10.1038/nn.3434.

712 McKnight D, Bean L, Karbassi I, Beattie K, Bienvenu T, Bonin H, Fang P, Chrisodoulou J, Friez
713 M, Helgeson M, et al. 2022. Recommendations by the ClinGen Rett/Angelman-like expert panel
714 for gene-specific variant interpretation methods. Hum Mutat. 43(8):1097–1113.
715 doi:10.1002/humu.24302.

716 McLaren W, Gil L, Hunt SE, Riat HS, Ritchie GRS, Thormann A, Flicek P, Cunningham F.
717 2016. The Ensembl Variant Effect Predictor. Genome Biol. 17(1):122. doi:10.1186/s13059-016-
718 0974-4.

719 Ng HH, Bird A. 1999. DNA methylation and chromatin modification. Curr Opin Genet Dev.
720 9(2):158–163. doi:10.1016/s0959-437x(99)80024-0.

721 Nomura Y. 2005. Early behavior characteristics and sleep disturbance in Rett syndrome. Brain
722 Dev. 27:S35–S42. doi:10.1016/j.braindev.2005.03.017.

723 Pascual-Alonso A, Martínez-Monseny AF, Xiol C, Armstrong J. 2021. MECP2-Related
724 Disorders in Males. Int J Mol Sci. 22(17):9610. doi:10.3390/ijms22179610.

725 Post KL, Belmadani M, Ganguly P, Meili F, Dingwall R, McDiarmid TA, Meyers WM,
726 Herrington C, Young BP, Callaghan DB, et al. 2020. Multi-model functionalization of disease-
727 associated PTEN missense mutations identifies multiple molecular mechanisms underlying
728 protein dysfunction. Nat Commun. 11(1):2073. doi:10.1038/s41467-020-15943-0.

729 Rodriguez JM, Maietta P, Ezkurdia I, Pietrelli A, Wesselink J-J, Lopez G, Valencia A, Tress
730 ML. 2013. APPRIS: annotation of principal and alternative splice isoforms. Nucleic Acids Res.
731 41(D1):D110–D117. doi:10.1093/nar/gks1058.

732 Schaaf CP, Sabo A, Sakai Y, Crosby J, Muzny D, Hawes A, Lewis L, Akbar H, Varghese R,
733 Boerwinkle E, et al. 2011. Oligogenic heterozygosity in individuals with high-functioning autism
734 spectrum disorders. Hum Mol Genet. 20(17):3366–3375. doi:10.1093/hmg/ddr243.

735 Skene PJ, Illingworth RS, Webb S, Kerr ARW, James KD, Turner DJ, Andrews R, Bird AP.
736 2010. Neuronal MeCP2 is expressed at near histone-octamer levels and globally alters the
737 chromatin state. Mol Cell. 37(4):457–468. doi:10.1016/j.molcel.2010.01.030.

738 Sperlazza MJ, Bilinovich SM, Sinanan LM, Javier FR, Williams DC. 2017. Structural Basis of
739 MeCP2 Distribution on Non-CpG Methylated and Hydroxymethylated DNA. J Mol Biol.
740 429(10):1581–1594. doi:10.1016/j.jmb.2017.04.009.

741 Syed A, Tainer JA. 2018. The MRE11–RAD50–NBS1 Complex Conducts the Orchestration of
742 Damage Signaling and Outcomes to Stress in DNA Replication and Repair. Annu Rev Biochem.
743 87(Volume 87, 2018):263–294. doi:10.1146/annurev-biochem-062917-012415.

744 Symington LS. 2002. Role of *RAD52* Epistasis Group Genes in Homologous Recombination and
745 Double-Strand Break Repair. Microbiol Mol Biol Rev. 66(4):630–670.
746 doi:10.1128/MMBR.66.4.630-670.2002.

747 Tillotson R, Bird A. 2020. The Molecular Basis of MeCP2 Function in the Brain. J Mol Biol.
748 432(6):1602–1623. doi:10.1016/j.jmb.2019.10.004.

749 Tong AH, Evangelista M, Parsons AB, Xu H, Bader GD, Pagé N, Robinson M, Raghibizadeh S,
750 Hogue CW, Bussey H, et al. 2001. Systematic genetic analysis with ordered arrays of yeast
751 deletion mutants. Science. 294(5550):2364–2368. doi:10.1126/science.1065810.

752 Vonhoff F, Williams A, Ryglewski S, Duch C. 2012. Drosophila as a model for MECP2 gain of
753 function in neurons. PloS One. 7(2):e31835. doi:10.1371/journal.pone.0031835.

754 Wan M, Lee SSJ, Zhang X, Houwink-Manville I, Song H-R, Amir RE, Budden S, Naidu S,
755 Pereira JLP, Lo IFM, et al. 1999. Rett Syndrome and Beyond: Recurrent Spontaneous and
756 Familial MECP2 Mutations at CpG Hotspots. Am J Hum Genet. 65(6):1520–1529.
757 doi:10.1086/302690.

758 Wang T, Guo H, Xiong B, Stessman HAF, Wu H, Coe BP, Turner TN, Liu Y, Zhao W,
759 Hoekzema K, et al. 2016. De novo genic mutations among a Chinese autism spectrum disorder
760 cohort. Nat Commun. 7(1):13316. doi:10.1038/ncomms13316.

761 Wang Y. 2014. RING finger protein 4 (RNF4) derepresses gene expression from DNA
762 methylation. J Biol Chem. 289(49):33808–33813. doi:10.1074/jbc.C114.611558.

763 Wen Z, Cheng T-L, Li G-Z, Sun S-B, Yu S-Y, Zhang Y, Du Y-S, Qiu Z. 2017. Identification of
764 autism-related MECP2 mutations by whole-exome sequencing and functional validation. Mol
765 Autism. 8:43. doi:10.1186/s13229-017-0157-5.

766 Williams AA, Mehler VJ, Mueller C, Vonhoff F, White R, Duch C. 2016. Apoptotic Activity of
767 MeCP2 Is Enhanced by C-Terminal Truncating Mutations. PLoS ONE. 11(7):e0159632.
768 doi:10.1371/journal.pone.0159632.

769 Williams AA, White R, Siniard A, Corneveaux J, Huentelman M, Duch C. 2016. MECP2
770 impairs neuronal structure by regulating KIBRA. Neurobiol Dis. 91:284–291.
771 doi:10.1016/j.nbd.2016.03.019.

772 Yang Y, Kucukkal TG, Li J, Alexov E, Cao W. 2016. Binding Analysis of Methyl-CpG Binding
773 Domain of MeCP2 and Rett Syndrome Mutations. ACS Chem Biol. 11(10):2706–2715.
774 doi:10.1021/acschembio.6b00450.

775 Young BP, Loewen CJR. 2013. Balony: a software package for analysis of data generated by
776 synthetic genetic array experiments. BMC Bioinformatics. 14:354. doi:10.1186/1471-2105-14-
777 354.

778 Young BP, Post KL, Chao JT, Meili F, Haas K, Loewen C. 2020. Sentinel interaction mapping -
779 a generic approach for the functional analysis of human disease gene variants using yeast. Dis
780 Model Mech. 13(7):dmm044560. doi:10.1242/dmm.044560.

781 Yusufzai TM, Wolffe AP. 2000. Functional consequences of Rett syndrome mutations on human
782 MeCP2. Nucleic Acids Res. 28(21):4172–4179.

783

784 **AUTHOR CONTRIBUTIONS**

785 DWA, CJRL, BPY, SMG, JTC, MD, SR, MD, PP contributed to conception of the work.

786 DWA, CJRL, GM, EC, BPY, SI, TL, JL, JBL, SMG, BB, MD, JS, SR, PP contributed to design

787 of the work.

788 DWA, CJRL, GM, EC, BPY, JBL, LM, JS, JBL, SR, PP contributed to acquisition, analysis, or

789 interpretation of data.

790 DWA, SR, PP, GM, EC, JBL, MD, KKC, BB, BW contributed to creation of new software used.

791 DWA, CJRL, JS, BPY, JTC, JBL, GM, EC, LM, JL, JBL, JTC, SR, PP contributed to drafting

792 the paper or substantively revised it.

793

794 **FIGURE CAPTIONS**

795 **Figure 1:** The forty-six MECP2 variants examined in this study. Domain locations of variants as
796 well as variant class, variant inheritance, and whether they are found in Rett Syndrome and/or
797 ASD. NTD – N-terminal domain, MBD – Methyl-CpG-binding domain, ID – Interdomain, TRD
798 – Transcription repressor domain, CTD – C-terminal domain.

799

800 **Figure 2:** MECP2 expression and effect on growth in yeast. (A) Untagged MECP2-ref expressed
801 from a 2-micron plasmid utilizing the estradiol-responsive promoter at various estradiol
802 concentrations in WT yeast. Equivalent amounts of yeast were loaded into each lane and western
803 blotted with anti-MECP2 antibody. M – molecular weight markers, arrowhead – full length
804 MECP2. (B) Effect of MECP2-ref expression on growth of WT yeast from a plasmid utilizing
805 the estradiol-responsive promoter at various estradiol concentrations. +EV – empty vector in
806 wild type yeast, +MECP2-ref – MECP2-ref plasmid in wild type yeast. (C) Similar to B except
807 using a 2-micron plasmid containing a galactose-responsive promoter and grown in galactose.
808 **** – indicates p value < 0.0001. ns – not significant.

809

810 **Figure 3:** Results of SIM genetic interaction screen with MECP2-ref. (A) Functional enrichment
811 for genetic interactions is shown where nodes indicate enriched GO terms and edges indicate
812 statistically significant associations between terms. Node size and edge thickness indicate
813 statistical significance (minimum $p < 0.05$, Bonferonni corrected). Highlighted labels indicate
814 most significant terms within networks. Network generated using Cytoscape and the ClueGO
815 plug-in. (B) Effect of MECP2-ref on yeast growth in mutants from the GO categories "DNA

816 damage response", "Chromatin organization" and "DNA binding" that were identified in the
817 SIM screen. Normalized colony size indicates the size of the colonies on the array plates after
818 accounting for the effect of MECP2-ref expression in WT yeast, in non-inducing (0 nM
819 estradiol) and inducing (10 nM estradiol) conditions.
820
821 **Figure 4:** Analysis of 46 MECP2 variants using the yeast assay. (A) Estimated functional effects
822 of MECP2 variants expressed in WT yeast. Data is normalized to MECP2-ref (=1) and empty
823 vector (=0). Error bars indicate 95% confidence intervals. (B) Protein stability of MECP2
824 variants in WT yeast. Protein levels were normalized to MECP2-ref and plotted on a log scale.
825 Error bars indicate S.D. (n = 3). * indicates $p < 0.05$, ** indicates $p < 0.01$. Colour coding same
826 as in (A). All variants are located in MBD except T228S (TRD), S356G (CTD) and P388S
827 (CTD).
828
829 **Figure 5:** *Drosophila* wing phenotypes induced by MECP2 variants. Representative images of
830 wings are shown expressing the indicated controls and variants. *attp40* – no MECP2, *MECP2-ref*
831 – WT MECP. All images are the same scale. Arrows indicate ectopic vein tissue for *UAS-*
832 *MECP2-ref* only.
833
834 **Figure 6:** Analysis of MECP2 variant wing vein phenotypes. We show our quantitation of total
835 wing vein per wing area for each genotype, normalized to *MECP2-ref* (WT MECP2) = 1 and
836 *attp40* (no MECP2) = 0. Error bars indicate 95% confidence intervals.

## SUPPLEMENTAL FIGURE CAPTIONS

**Supplemental Figure 1**: Representative MECP2 Western blots. Arrow indicates the full-length MECP2 protein. Antibody labelling is as follows: red - anti-MECP2, green - anti-PGK1.

**Supplemental Figure 2**: Representative wing phenotypes for control, benign and pathogenic MECP2 calibration variants tested in *Drosophila*. For each variant, raw images are on the left and the masked image used to quantitate total wing vein per wing is on the right.

**Supplemental Figure 3**: Representative wing phenotypes for test (ASD) MECP2 variants tested in *Drosophila*. For each variant, raw images are on the left and the masked image used to quantitate total wing vein per wing is on the right.

## SUPPLEMENTAL METHODS CAPTIONS

**Supplemental Methods 1:** Detailed outline of wing vein quantitation methods.

**Supplemental Methods 2:** Yeast statistical model R script.

**Supplemental Methods 3:** Fly statistical model R script.

## SUPPLEMENTAL TABLE CAPTIONS

**Supplemental Table 1:** MECP2 protein stability summary table.

## SUPPLEMENTAL DATA CAPTIONS

**Supplemental Data 1:** Detailed information for each variant, primers used in cloning, the molecular genetic reagents made for each organism, and the *Drosophila* stocks generated.

**Supplemental Data 2:** Yeast SIM screen raw data.

**Supplemental Data 3:** GO analysis results for yeast SIM screen listing genes in each GO term.

**Supplemental Data 4:** Raw data for yeast variant assays used in statistical model.

**Supplemental Data 5:** Raw data for *Drosophila* variant assays used in statistical model.

# Figure 1

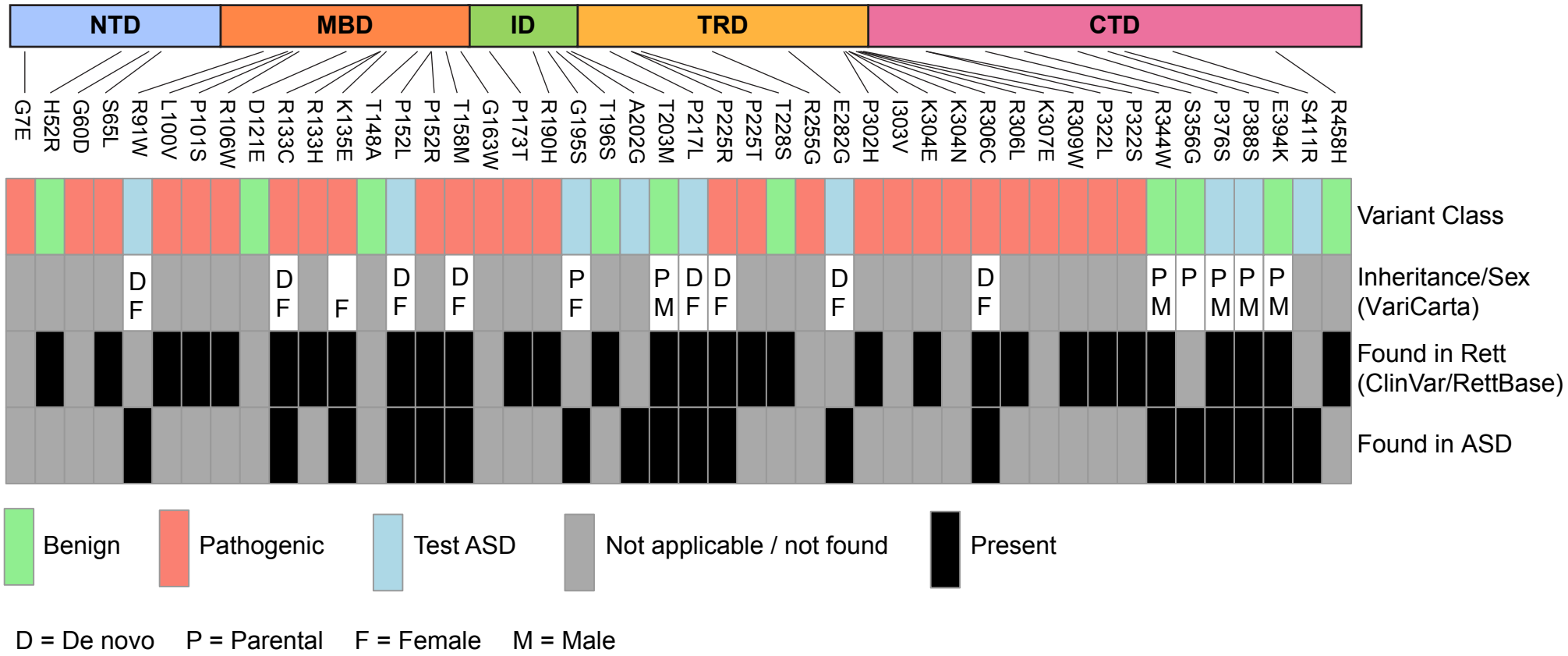
NTD
MBD
ID
TRD
CTD
G7E
H52R
G60D
S65L
R91W
L100V
P101S
R106W
D121E
R133C
R133H
K135E
T148A
P152L
P152R
T158M
G163W
P173T
R190H
G195S
T196S
A202G
T203M
P217L
P225R
P225T
T228S
R255G
E282G
P302H
I303V
K304E
K304N
R306C
R306L
K307E
R309W
P322L
P322S
R344W
S356G
P376S
P388S
E394K
S411R
R458H
Variant Class
Inheritance/Sex (VariCarta)
Found in Rett (ClinVar/RettBase)
Found in ASD
Benign
Pathogenic
Test ASD
Not applicable / not found
Present
D = De novo
P = Parental
F = Female
M = Male

# Figure 2

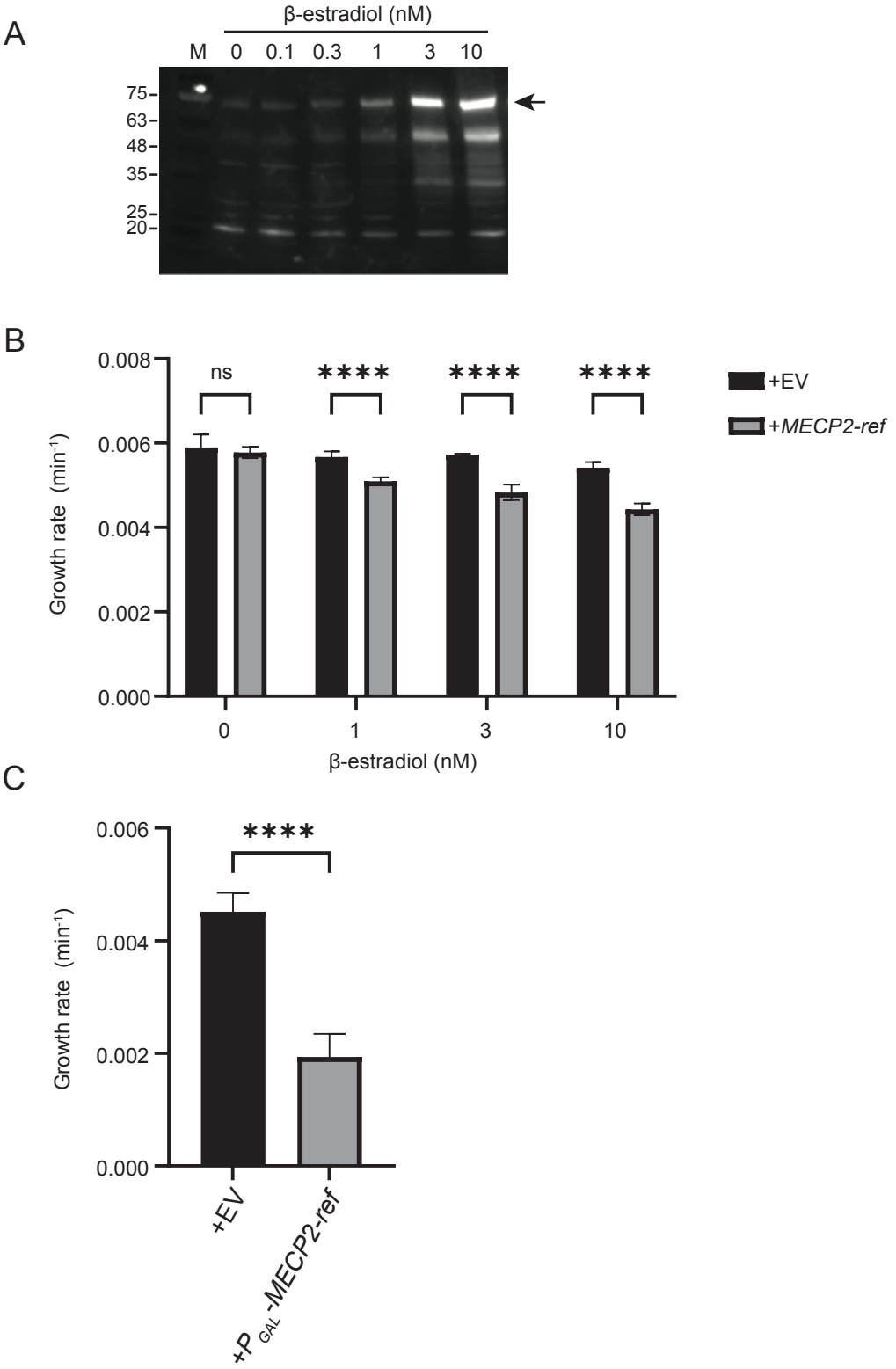
A
β-estradiol (nM)
M 0 0.1 0.3 1 3 10
75
63
48
35
25
20
B
0.008
0.006
0.004
0.002
0.000
Growth rate (min-1)
ns
****
****
****
+EV
+MECP2-ref
0
1
3
10
β-estradiol (nM)
C
0.006
0.004
0.002
0.000
Growth rate (min-1)
****
+EV
+P GAL -MECP2-ref

# Figure 3

A

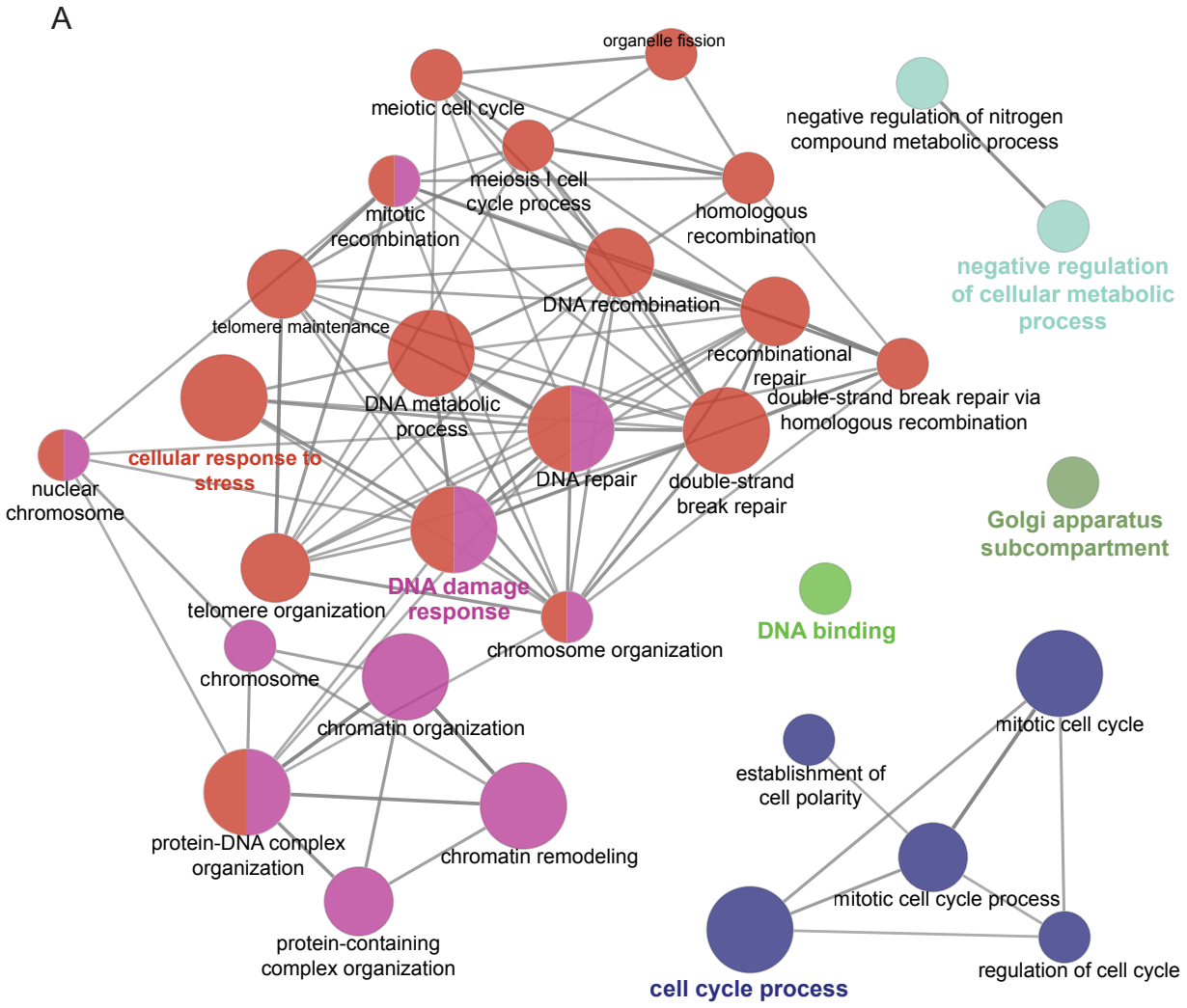
organelle fission
meiotic cell cycle
negative regulation of nitrogen compound metabolic process
meiosis I cell cycle process
mitotic recombination
homologous recombination
negative regulation of cellular metabolic process
DNA recombination
telomere maintenance
recombinational repair
double-strand break repair via homologous recombination
DNA metabolic process
cellular response to stress
nuclear chromosome
DNA repair
double-strand break repair
Golgi apparatus subcompartment
DNA damage response
telomere organization
DNA binding
chromosome organization
chromosome
chromatin organization
mitotic cell cycle
establishment of cell polarity
protein-DNA complex organization
chromatin remodeling
mitotic cell cycle process
protein-containing complex organization
regulation of cell cycle
cell cycle process

B

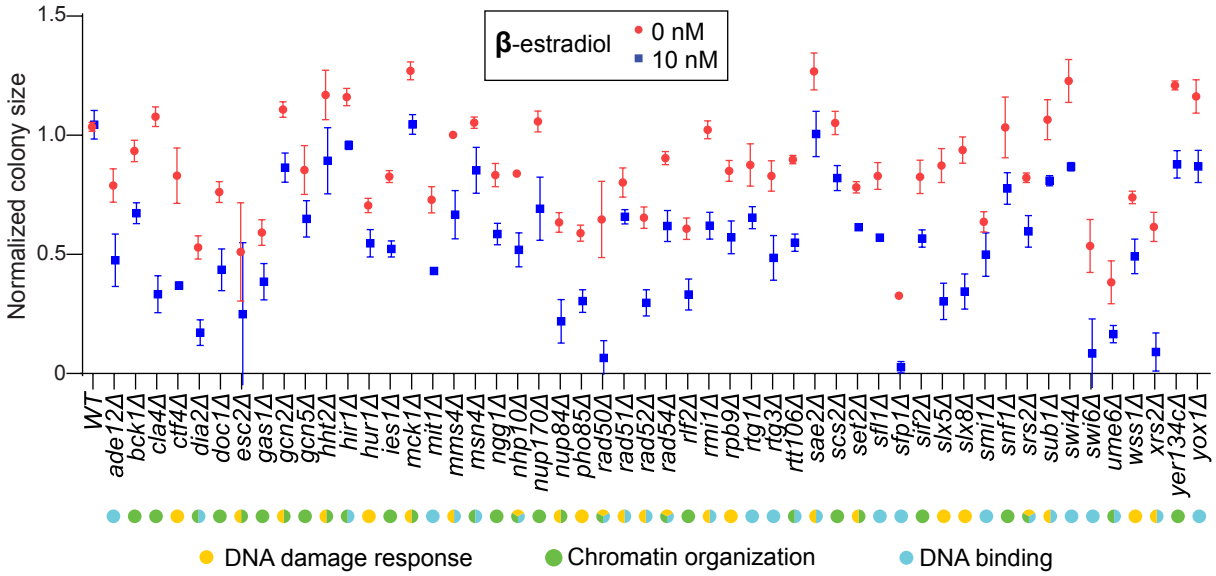
β-estradiol
0 nM
10 nM
Normalized colony size
1.5
1.0
0.5
0
WT
ade12Δ
bck1Δ
cla4Δ
ctf4Δ
dia2Δ
doc1Δ
esc2Δ
gas1Δ
gcn2Δ
gcn5Δ
hht2Δ
hir1Δ
hur1Δ
ies1Δ
mck1Δ
mit1Δ
mms4Δ
msn4Δ
ngg1Δ
nhp10Δ
nup170Δ
nup84Δ
pho85Δ
rad50Δ
rad51Δ
rad52Δ
rad54Δ
rif2Δ
rmi1Δ
rpb9Δ
rtg1Δ
rtg3Δ
rtt106Δ
sae2Δ
scs2Δ
set2Δ
sfi1Δ
sfp1Δ
sir2Δ
slx5Δ
slx8Δ
smi1Δ
snf1Δ
srs2Δ
sub1Δ
swi4Δ
swi6Δ
ume6Δ
wss1Δ
xrs2Δ
yer134cΔ
yox1Δ
DNA damage response
Chromatin organization
DNA binding

# Figure 4

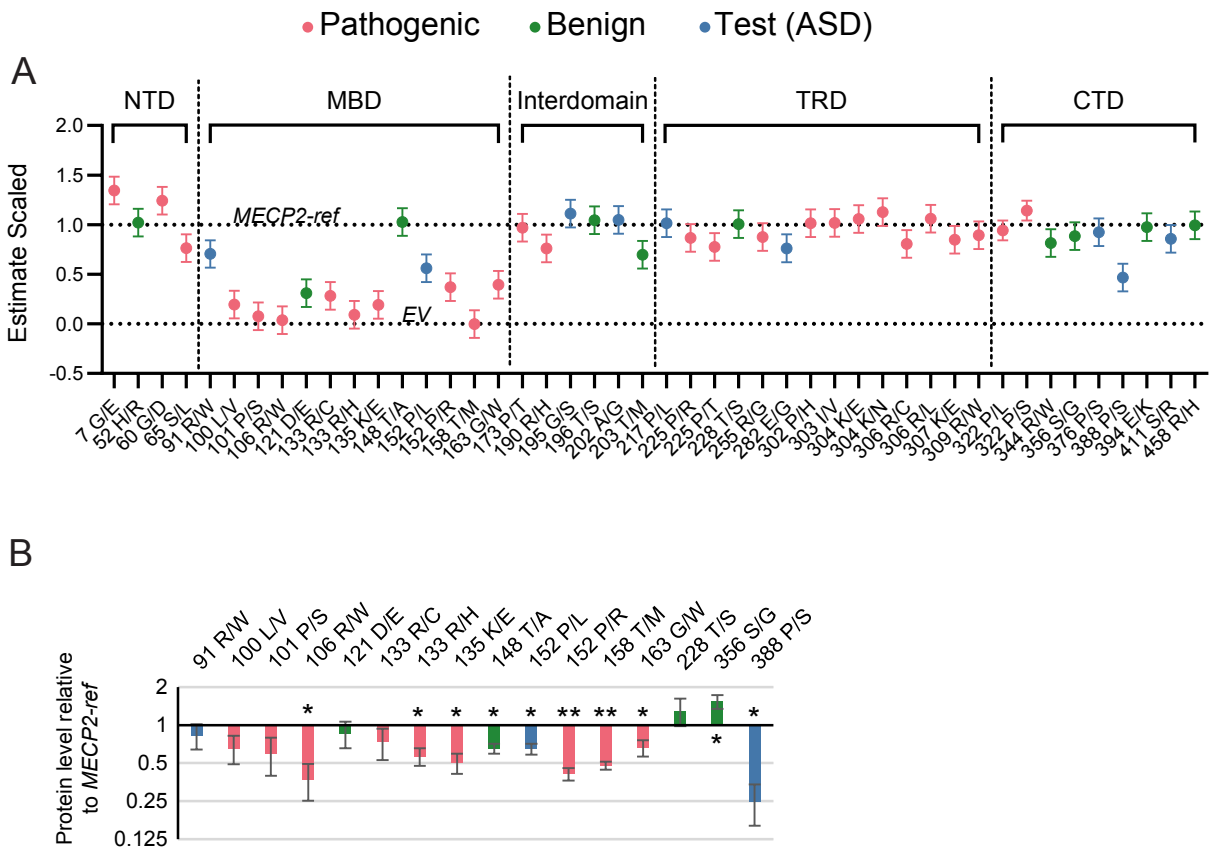
Pathogenic
Benign
Test (ASD)
A
NTD
MBD
Interdomain
TRD
CTD
Estimate Scaled
2.0
1.5
1.0
0.5
0.0
-0.5
MECP2-ref
EV
7 G/E
52 H/R
60 G/D
65 S/L
91 R/W
100 L/V
101 P/S
106 R/W
121 D/E
133 R/C
133 R/H
135 K/E
148 T/A
152 P/L
152 P/R
158 T/M
163 G/W
173 P/T
190 R/H
195 G/S
196 T/S
202 A/G
203 T/M
217 P/L
225 P/R
225 P/T
228 T/S
255 R/G
282 E/G
302 P/H
303 I/V
304 K/E
304 K/N
306 R/C
306 R/L
307 K/E
309 R/W
322 P/L
322 P/S
344 R/W
356 S/G
376 P/S
388 P/S
394 E/K
411 S/R
458 R/H
B
91 R/W
100 L/V
101 P/S
106 R/W
121 D/E
133 R/C
133 R/H
135 K/E
148 T/A
152 P/L
152 P/R
158 T/M
163 G/W
228 T/S
356 S/G
388 P/S
Protein level relative to MECP2-ref
2
1
0.5
0.25
0.125
*
*
*
*
*
**
**
*
*
*

# Figure 5

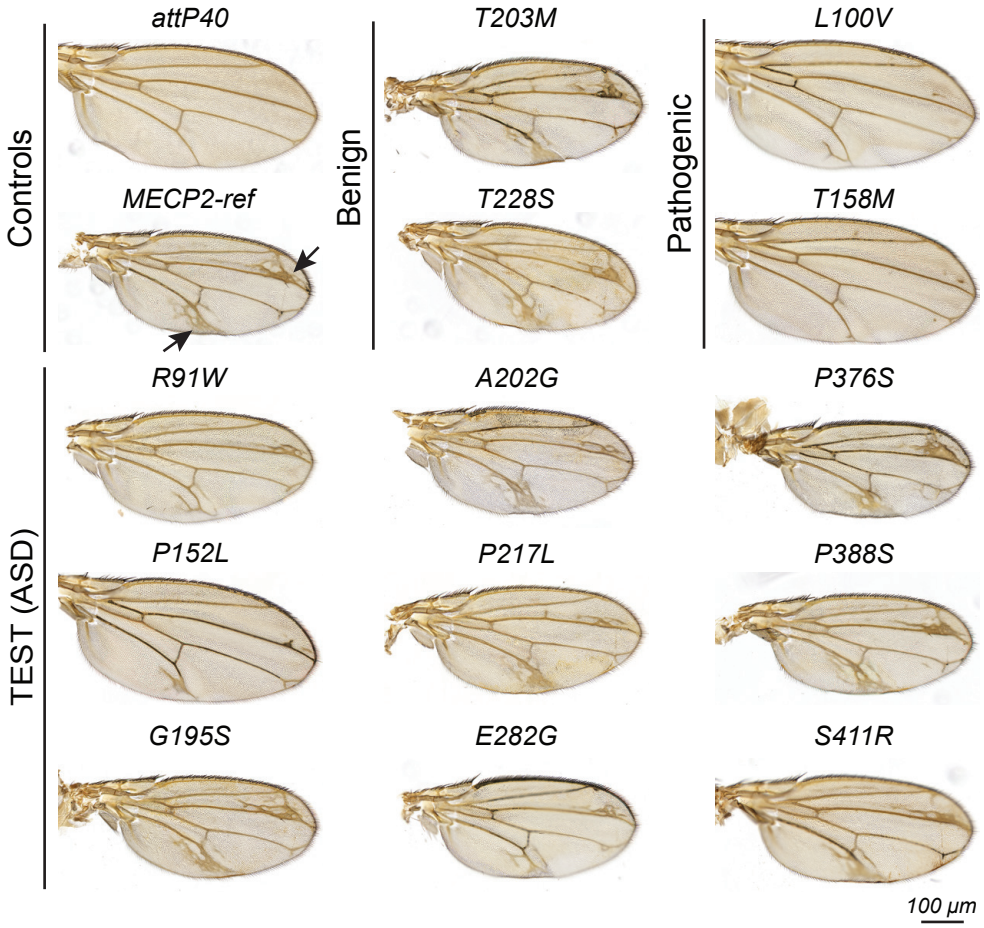
Controls
attP40
MECP2-ref
Benign
T203M
T228S
Pathogenic
L100V
T158M
TEST (ASD)
R91W
A202G
P376S
P152L
P217L
P388S
G195S
E282G
S411R
100 µm

# Figure 6

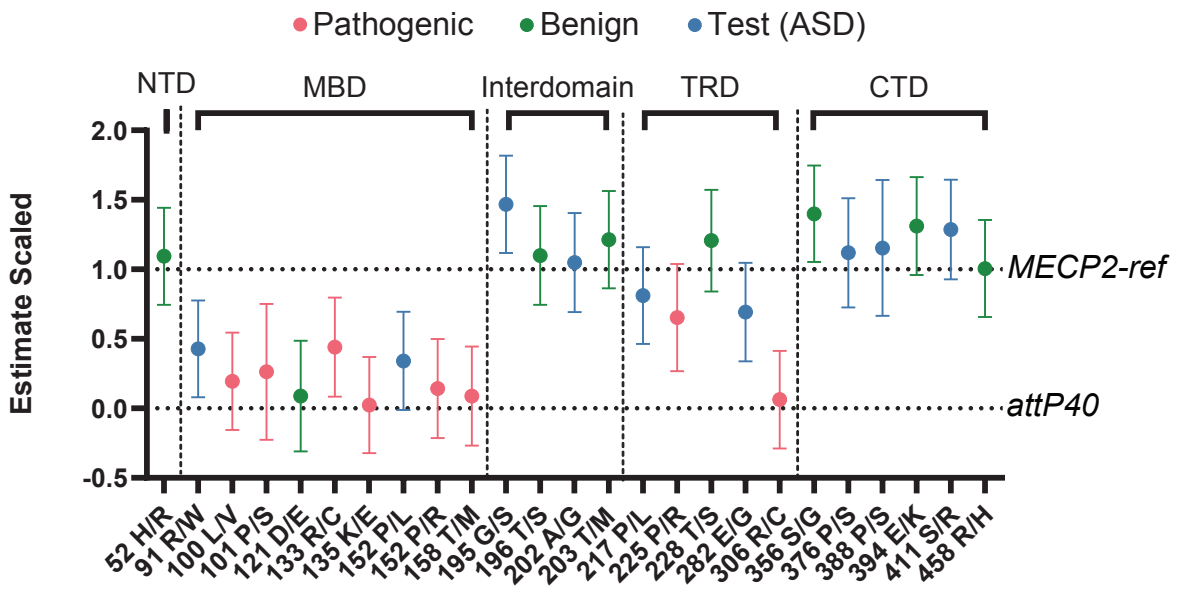
Pathogenic
Benign
Test (ASD)
NTD
MBD
Interdomain
TRD
CTD
Estimate Scaled
2.0
1.5
1.0
0.5
0.0
-0.5
MECP2-ref
attP40
52 H/R
91 R/W
100 L/V
101 P/S
121 D/E
133 R/C
135 K/E
152 P/L
152 P/R
158 T/M
195 G/S
196 T/S
202 A/G
203 T/M
217 P/L
225 P/R
228 T/S
282 E/G
306 R/C
356 S/G
376 P/S
388 P/S
394 E/K
411 S/R
458 R/H

# Supplemental Figure 1

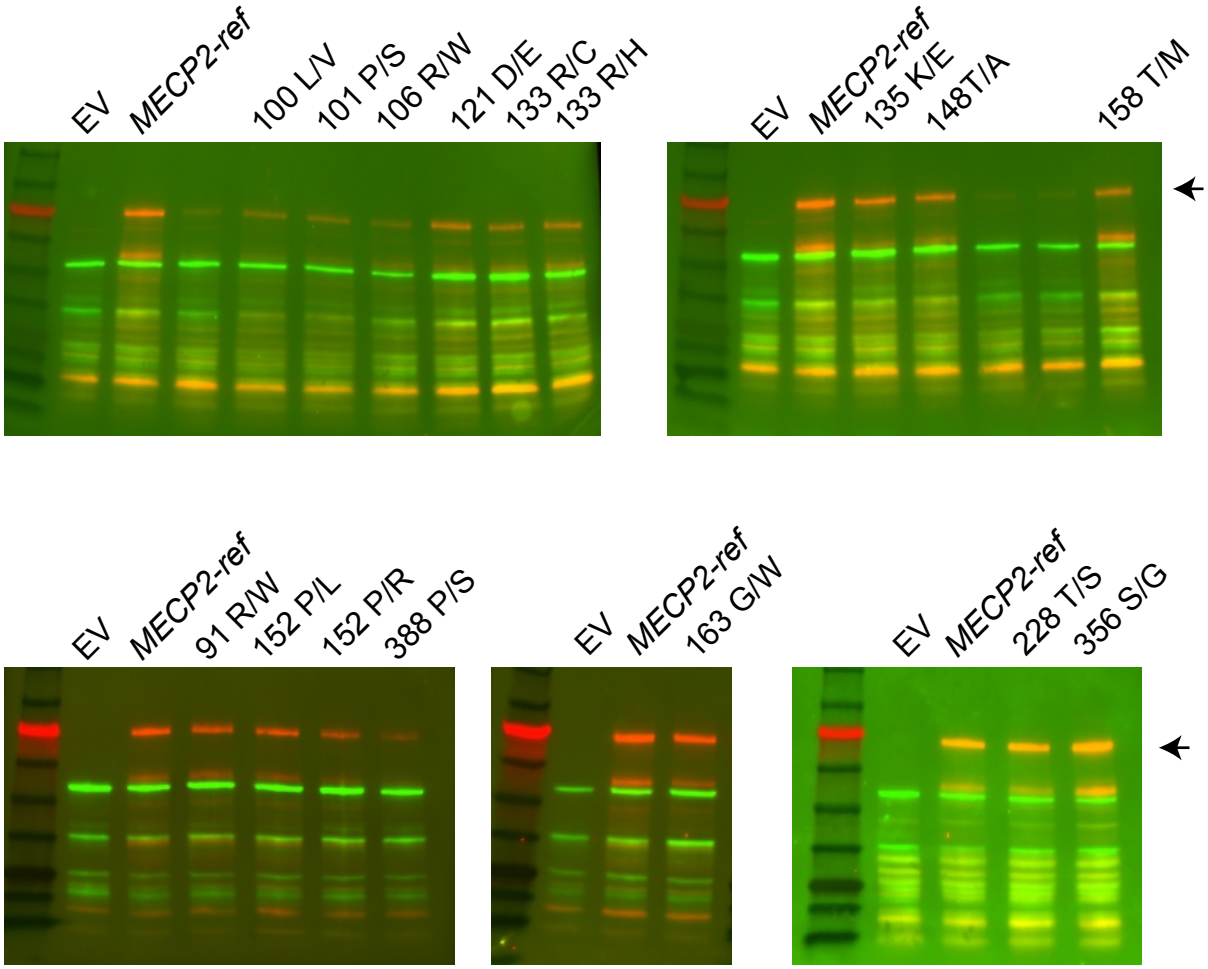

# Supplemental Figure 2

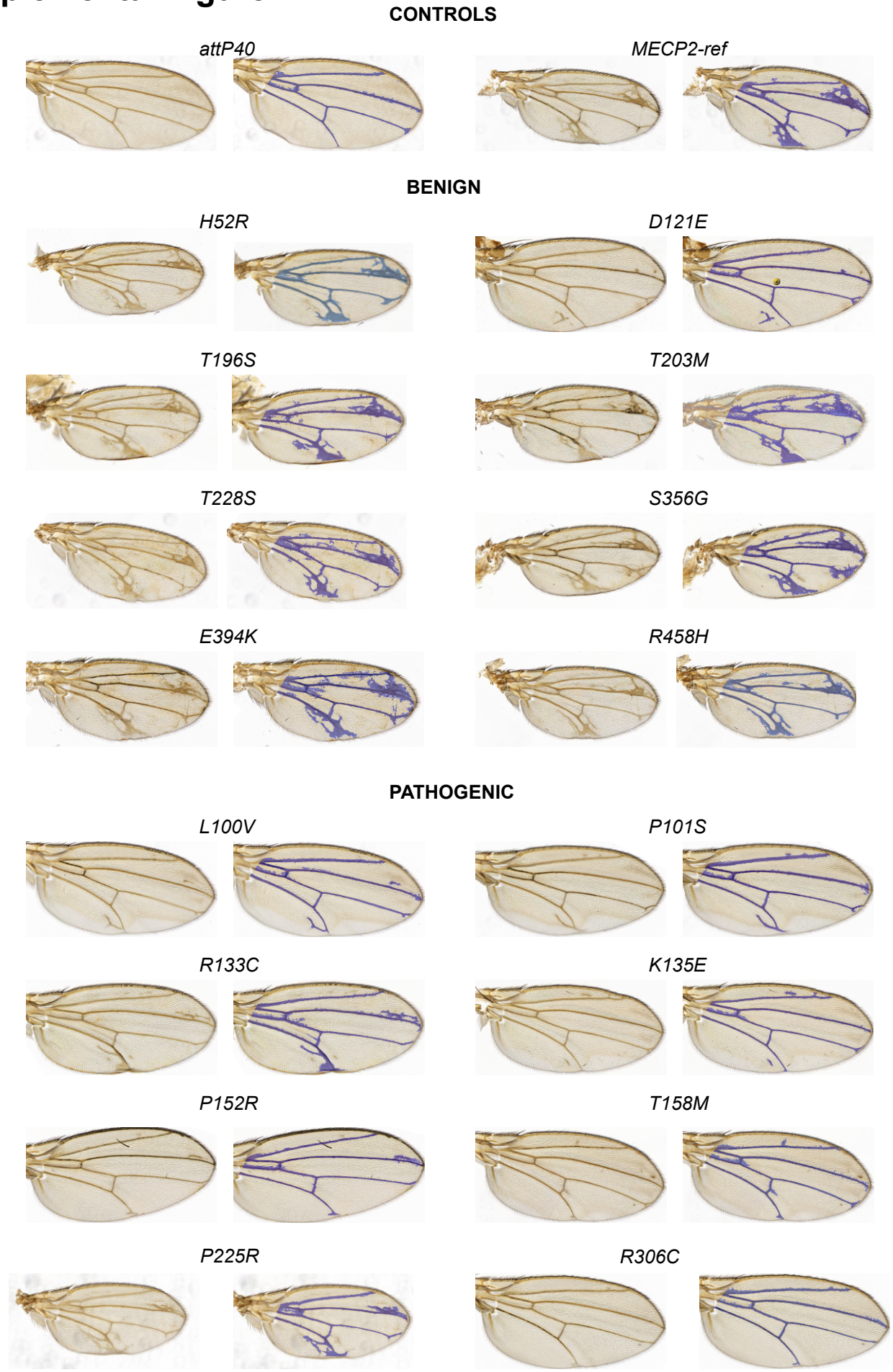

# Supplemental Figure 3

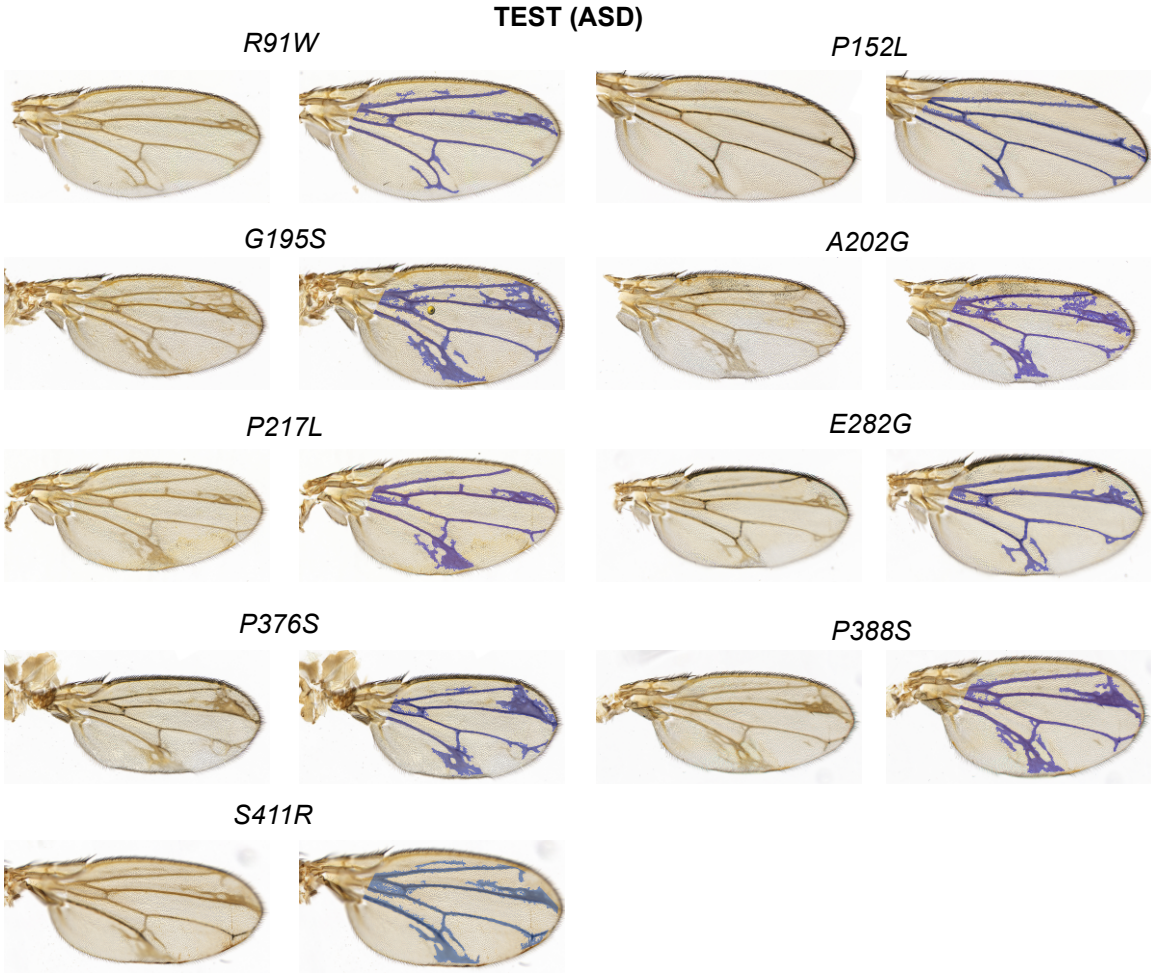

Supplemental Table 1: Summary of MECP2 protein stability results

| Variant | Yeast* (this study) | Yang [1] (in vitro, WT = 1) | Kucukkal [2] (in vitro) (ΔΔG) | Sperlazza [3] (NMR) (+ slight, ++ more destabilized) | Tillotson [4] (mouse models, WT = 1) |
|---|---|---|---|---|---|
| R91W | 1 | | | | |
| L100V | 1 | 0.5 | +1.25 | | |
| P101S | 1 | | | + | |
| R106W | 0.37 | 1 | +0.1 | ++ | 0.1 (TAVI) |
| D121E | 1 | | | | |
| R133C | 1 | 1 | +0.4 | | 0.6 (eGFP) |
| R133H | 0.56 | 1 | +0.25 | | |
| K135E | 0.50 | | | | |
| T148A | 0.65 | | | | |
| P152L | 0.65 | | | | |
| P152R | 0.41 | 0.25 | +1.5 | | |
| T158M | 0.48 | 1 | +0.25 | + | 0.3 (eGFP), 0.25 (TAVI) |
| G163W | 0.66 | | | | |
| P225R | | | | | 0.22 |
| T228S | 1 | | | | |
| R306C | | | | | 1.0 |
| P322L | | | | | 0.03 |
| S356G | 1.54 | | | | |
| P388S | 0.25 | | | | |

* Values not significantly different than MECP2-Ref are set to 1, all others are significant ($p<0.05$)


References:

1. Yang, Y., Kucukkal, T. G., Li, J., Alexov, E. & Cao, W. Binding Analysis of Methyl-CpG Binding Domain of MeCP2 and Rett Syndrome Mutations. *ACS Chem. Biol.* **11**, 2706–2715 (2016).
2. Kucukkal, T. G., Yang, Y., Uvarov, O., Cao, W. & Alexov, E. Impact of Rett Syndrome Mutations on MeCP2 MBD Stability. *Biochemistry* **54**, 6357–6368 (2015).
3. Sperlazza, M. J., Bilinovich, S. M., Sinanan, L. M., Javier, F. R. & Williams, D. C. Structural Basis of MeCP2 Distribution on Non-CpG Methylated and Hydroxymethylated DNA. *J. Mol. Biol.* **429**, 1581–1594 (2017).
4. Tillotson, R. & Bird, A. The Molecular Basis of MeCP2 Function in the Brain. *J. Mol. Biol.* **432**, 1602–1623 (2020).